Article
Vol. 27, No. 6, p. 711–733, December 2023
https://doi.org/10.1007/s12303-023-0023-8
pISSN 1226-4806 eISSN 1598-7477
Geosciences Journal GJ

Assessment of the relative tectonic activity of the Longxian-Baoji Fault Zone in the northeastern Tibetan Plateau based on geomorphic indices

Qi Huang[1], Xiaohu Zhou[1]*, Jiyuan You[2], Shuaishuai Xu[1], Lushan Liu[1], and Yang Wang[1]

[1]Department of Geology, State Key Laboratory of Continental Dynamics, Northwest University, No. 229, Northern Taibai Road, Beilin District, Xian 710069, China
[2]School of Energy and Engineering, Yulin University, No. 51, Chongwen Road, Yuyang District, Yulin 719000, China

ABSTRACT: Since the Late Cenozoic, tectonic deformation has been intense in the Longxian–Baoji Fault Zone (LBFZ), which is at the intersection of the southwest margin of the Ordos Block, the northeast margin of the Tibet Plateau, and the Qinling Orogenic Belt. To evaluate the relative tectonic activity within the LBFZ and discuss the influence of the northeastward expansion of the Tibetan Plateau on the geomorphological evolution of the LBFZ, we extracted data of the Qianhe, Hengshuihe, and Jinlinghe River Basins from the ASTER GDEM and analyzed the geomorphic indices, including the hypsometric integral (HI), standardized stream length-gradient index (SL/K) and Hack profile, elongation ratio (Re), the drainage basin asymmetry factor (AF) and valley floor width-to-height ratio (VF). Through geomorphic indices and field investigations, we found that the LBFZ has experienced relatively high tectonic activity. Combined with the index of relative active tectonics (IAT), we compared the tectonic activity strengths of the four major faults in the study area. Among them, the tectonic activities of the Longxian-Qishan Fault (LQF) and the Taoyuan-Guichuansi Fault (TGF) are the highest. The morphology and AF values of the drainage basin of the southwest side of the study area indicate the influence of northwest-southeast compressive stress. The northeastward expansion of the Tibetan Plateau affected the LBFZ region, and the stress brought about by it controlled the tectonic deformation in the region and sculpted the modern landscape. This study is of great significance for understanding the impact of the northeastward expansion of the Tibetan Plateau on the geomorphological evolution of the LBFZ.

Key words: geomorphic indices, Longxian–Baoji Fault Zone, northeastern Tibetan Plateau, southwest margin of Ordos, tectonic activity

Manuscript received January 9, 2023; Manuscript accepted June 27, 2023

1. INTRODUCTION

Tectonic geomorphology is an emerging interdisciplinary field between geomorphology, geodynamics, and structural geology, which focuses on the interactions between tectonic and surface processes (Wang and Wang, 2005; Burbank and Anderson, 2012; Liu et al., 2018). It is an important means for studying the internal and external dynamic coupled system of the Earth. The main factors that influence landform evolution include climate, topography, lithology, and tectonics. Tectonic activities can directly or indirectly control geomorphic evolution (Bull, 2007, 2009; Figueiredo et al., 2019). Tectonic geomorphology began to emerge in the mid-20th century with the development of neotectonic activity studies and the birth of plate tectonic theory (Wang and Wang, 2005). Since the 1990s, with the rapid development and application of new dating techniques and spatial exploration methods, especially the introduction of the digital elevation model (DEM), tectonic geomorphology has ushered in a rapid development opportunity and entered a new stage of quantitative research. It has achieved remarkable results in determining the height of the original geomorphic surface, the amplitude and rate of tectonic activity, the erosion rate, and

Editorial responsibility: Raehee Han

***Corresponding author:**
Xiaohu Zhou
Department of Geology, State Key Laboratory of Continental Dynamics, Northwest University, No. 229, Northern Taibai Road, Beilin District, Xian 710069, China
Tel: +86-13759922479, E-mail: zhouxiaohu@nwu.edu.cn

Electronic supplementary material
The online version of this article (https://doi.org/10.1007/s12303-023-0023-8) contains supplementary material, which is available to authorized users.

the balance between tectonic uplift and erosion downcutting. Tectonic geomorphology has become an international research hotspot and has shown broad application prospects in the fields of disaster evaluation, environmental and climate change, and neotectonic evolution (Cheng et al., 2016; Ghosh and Sivakumar, 2018; Liu et al., 2018; Gimenez et al., 2022). DEM is a discrete mathematical expression and simulation of the Earth's surface (Summerfield, 2000), which can quantitative description the geomorphological characteristics of drainage basins by analyzing the geomorphic indices, and enables better and faster analyze the topographic changes caused by the interaction between tectonic and surface processes (Farr and Kobrick, 2000; Grohmann, 2004; Troiani and Della Seta, 2008; Azañón et al., 2012). Quantitative analyses of geomorphic indices have become powerful tools for the study of tectonics and have been successfully incorporated into many studies (e.g., Keller and Rockwell, 1984; Keller et al., 2002; Gao et al., 2013; Chang et al., 2014; Dar et al., 2014; Domínguez-González et al., 2015; Dai et al., 2016; Faghih et al., 2016; Cheng et al., 2018; Shi et al., 2020; Erbello et al., 2022).

The uplift of the Tibetan Plateau (Fig. 1a), which is commonly referred to as the roof of the world, is the most important geological event in Asia in modern times. It took place in the Early Cenozoic (about 55 Ma) as a result of the collision and continuous compression and uplift of the Indian and Eurasian plates (Molnar and Tapponnier, 1975; Yin and Harrison, 2000; Tapponnier et al., 2001) and is a natural laboratory for the study of continental dynamics (Meyer et al., 1998; Tapponnier et al., 2001; Pei et al., 2021; Yang, Y.H. et al., 2022; Zhang et al., 2022). It has fundamental impacts on the atmospheric circulation of East Asia and the geological evolution of the continent of Asia as well as other parts of the planet (Zhisheng et al., 2001; Royden et al., 2008; Fang, 2017). It contributed to the transformation of the topography of China in which the positive elevation gradient from west to east was replaced by one from east to west. The uplift and expansion of the Tibetan Plateau created extremely large northeast-southwest compressive stresses towards the northeast, which resulted in substantial uplift of the surrounding tectonic units and the existed of numerous active strike-slip and thrust faults on the northeast margin of the Tibetan Plateau (Peltzer et al., 1989; Zhang et al., 1991; Meyer et al., 1998; Zhang et al., 2004). Studies of the tectonic geomorphology, tectonic activity, and dynamics of this region are important for our understanding of the expansion of the northeast margin of the Tibetan Plateau.

The Longxian–Baoji Fault Zone (LBFZ) is at the intersection of the northeast margin of the Tibetan Plateau, the southwest margin of the Ordos Block, and the Qinling Orogen. It is the most leading edge of the northeastward expansion of the Tibetan Plateau after the collision between the Indian and Eurasian plates (Yuan et al., 2004, 2013; Zheng et al., 2013, 2016; Li, 2017; Fan et al., 2020; Wang et al., 2021). Because of the unique tectonic location of the LBFZ, the area has strong tectonic activity and has been prone to earthquakes in China. The LBFZ is mainly composed of four northwest-southeast trending normal faults that form a wedge-shaped. The LBFZ has been the subject of many studies, which have focused on fault geometry, tectonic stress, and sliding rate (e.g., Sun and Deng, 1994; Liu et al., 1997; Guo et al., 2012; Tang et al., 2015; Li, X.N. et al., 2018; Li, Y.H. et al., 2018; Dai and Tang, 2021; Wang et al., 2021). In recent years, scholars have begun to study the tectonic geomorphology of the LBFZ. For example, Zhang et al. (2019) discussed the activity of the Qianhe River Basin through the analysis of geomorphic indices. Liu et al. (2020) evaluated the geomorphological response of the +Qianhe River Basin to active faults through river longitudinal profiles and knickpoints. Fan et al. (2020) quantitatively analyzed the tectonic geomorphological features and activity of the Longxian-Qishan Fault (LQF) through geomorphic indices. However, the above studies mainly focused on the Qianhe River Basin or the LQF and don't have a good overall interpretation of the LBFZ. Therefore, as a supplement to previous studies, we examined the geomorphic indices of the Qianhe, Hengshuihe, and Jinlinghe River Basins on the southwest margin of the Ordos block based on DEM. The main purpose of this study is to evaluate relative tectonic activity within the LBFZ and discuss the influence of the northeastward expansion of the Tibetan Plateau on the geomorphological evolution of the LBFZ.

2. REGIONAL SETTING

2.1. Geomorphology

The LBFZ is on the northwest margin of the Weihe Graben. Figure 1b shows the general topographic features of the study area. Elevation varies from 400m to 3300m, and the overall topography of the area is high in the west and low in the east. The Weihe Graben is relatively low and flat, but the topography within the LBFZ is steep and has a maximum elevation of about 1500 m. Figure 1c and Figure 1d are maps of the swath topographic profile (A–A' and B–B') and show the maximum, mean, and minimum elevations along 5 and 6 km wide swaths centered on the cross-section lines shown, respectively. They show a series of steep slopes and deeply incised V-shaped valleys, which indicate relatively recent tectonic activity.

Qianhe River, Hengshuihe River, and Jinlinghe River are the three drainage systems in the LBFZ (Fig. 2b). Qianhe River is the longest, has the largest drainage area, and is the largest tributary of Weihe River in the area. Almost all the tributaries of the three drainage systems are perpendicular to the fault, and

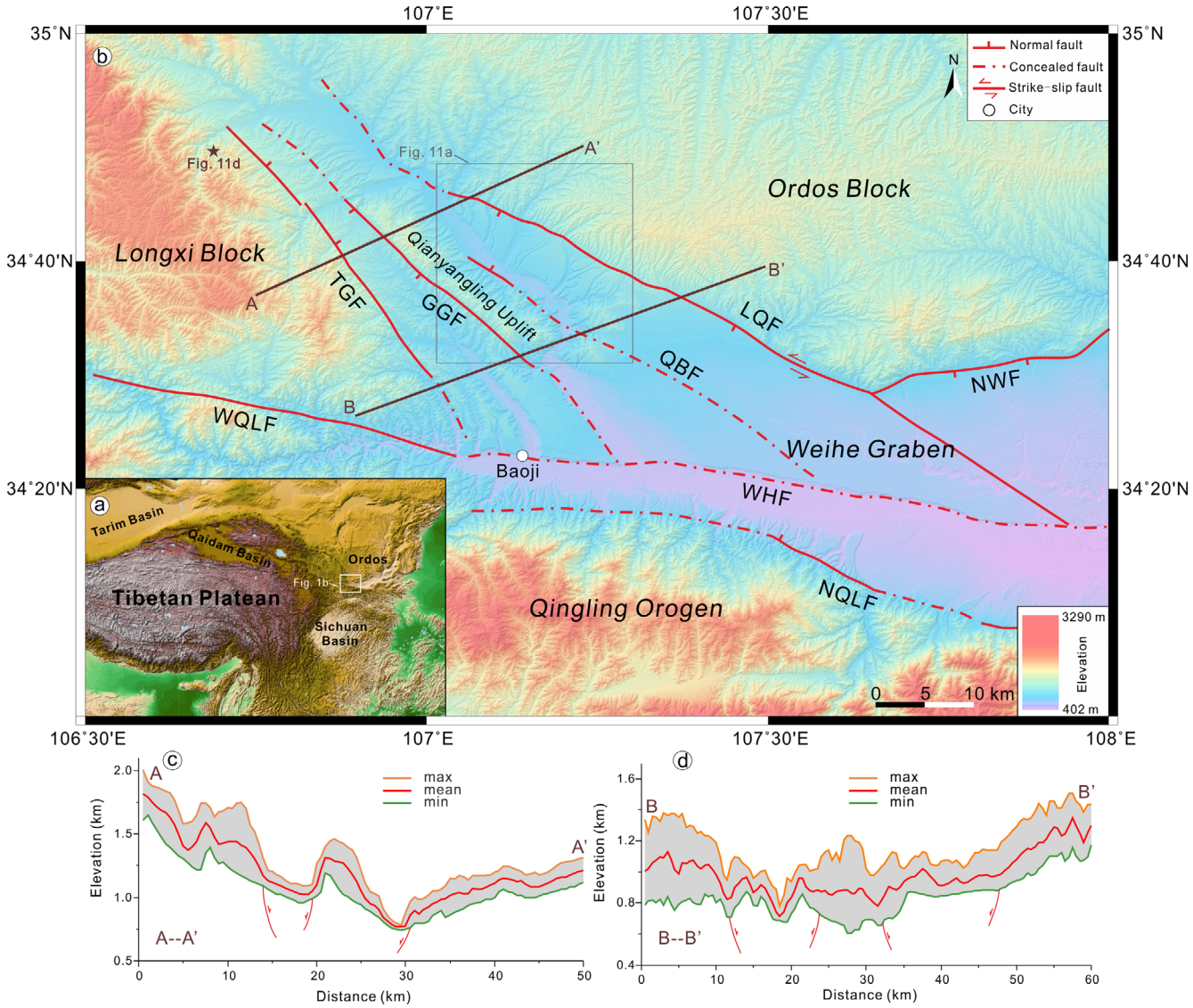

Fig. 1. Regional topographic characteristics. (a) Regional topographic map of the Tibetan Plateau (From http://www.data.ac.cn/map/mi887); (b) Regional geomorphic and active fault distribution map. GGF: Guguan-Guozhen Fault; LQF: Longxian-Qishan Fault; NQLF: Northern Qinling Fault; WHF: Weihe Fault; NWF: Northern Weihe Fault; QBF: Qianyang-Biaojiao Fault; TGF: Taoyuan-Guichuansi Fault; WQLF: Western Qinling Fault. The source of the active faults is referenced from Li et al. (2004) and Li et al. (2019). (c and d) Swath topographic profile (A–A′ and B–B′) and show the maximum, mean, and minimum elevations along 5 and 6 km wide swaths centered on the cross-section lines shown, respectively.

very few tributaries are parallel to it.

2.2. Regional Geology

The LBFZ lies on the northeast margin of the Tibetan Plateau and the southwest margin of the Ordos block. It runs from Longxian in the north to Baoji in the south. It is composed of four main northwest-southeast trending faults. From west to east, they are the Taoyuan-Guichuansi Fault (TGF), the Guguan-Guozhen Fault (GGF), the Qianyang-Biaojiao Fault (QBF), and the Longxian-Qishan Fault (LQF) (Fig. 2a). Together, they control the tectonic framework of the drainage basin (Chen, Q.Y. et al., 2018; Zhang et al., 2019; Liu et al., 2020). The LBFZ is bounded by the Weihe Fault in the south. It is wedge-shaped (Li, X.N. et al., 2018) and narrower in the northwest (width of 15 km) and wider in the southeast (width of 70 km) (Fig. 2a). Fault spacing increases from northwest to southeast.

These four faults have been in an alternating horst-graben arrangement since the Early Cretaceous (State Seismological Bureau Research Group (SSBRG), 1988; Zhang et al., 2017; Wang, S.D. et al., 2018; Dai and Tang, 2021). The LBFZ has been uplifting since the Late Mesozoic. Aeolian loess from the Miocene to Quaternary is dominant and Late Cretaceous–Oligocene deposits are missing (SSBRG, 1988; Bureau of Geology and

https://doi.org/10.1007/s12303-023-0023-8

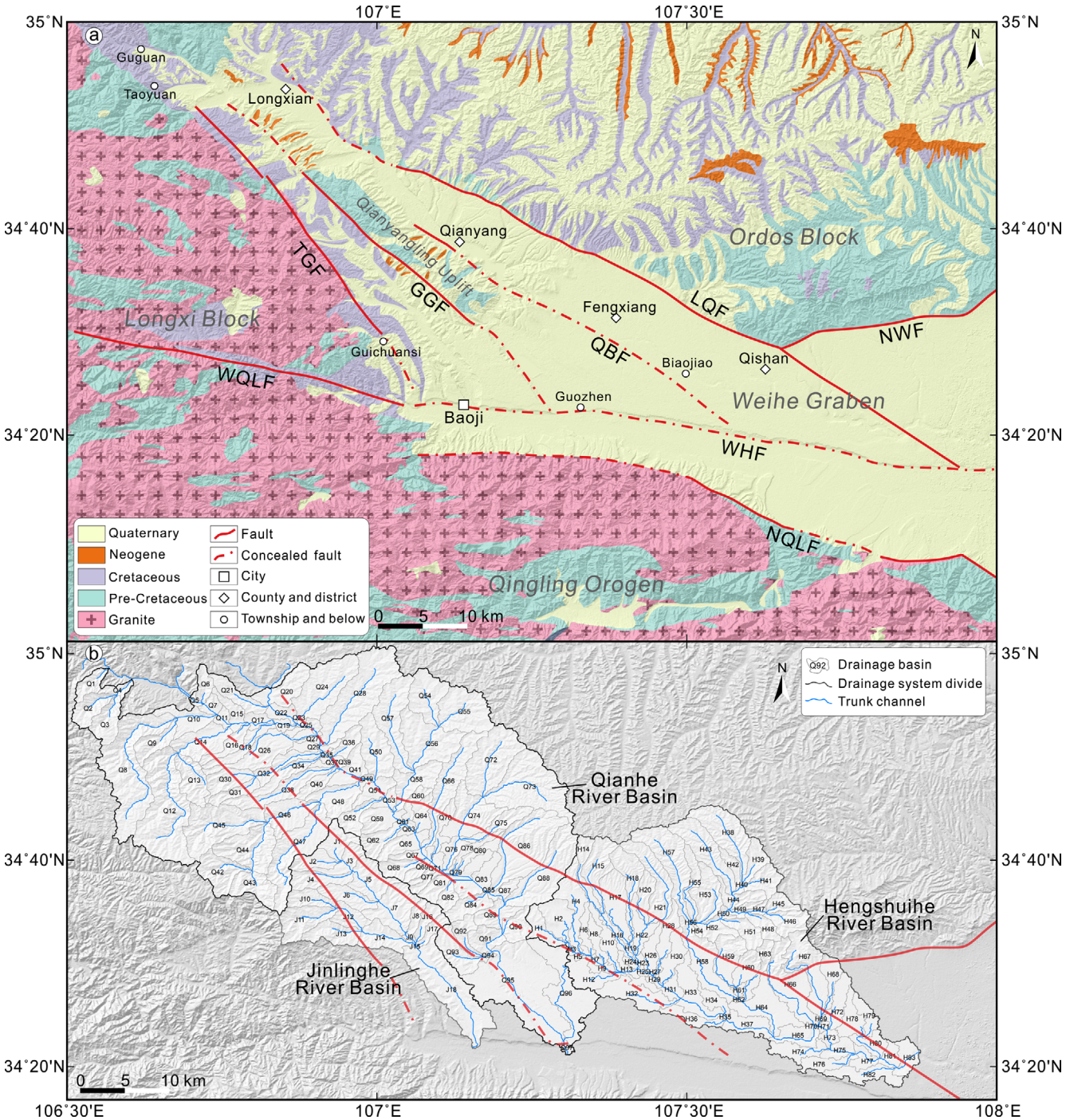

Fig. 2. (a) Simplified geological map of the study area, modified from 1:250,000 geological map of Baoji (Li et al., 2004). Among them, the lithology of the Quaternary is loess, the lithology of the Neogene is clay, the lithology of the Cretaceous is sandstone and conglomerate, and the lithology of the pre-Cretaceous is sandstone, limestone, dolomite, marble, and gneiss. (b) Distribution map of the drainage basins extracted within the LBFZ.

Mineral Resources of Shaanxi Province, 1989; Zhang et al., 2017; Wang et al., 2021). During the Quaternary and the uplift of the Tibetan Plateau, the Longxi block on the west side of the LBFZ rotated clockwise and the Ordos block on the east side of the LBFZ rotated counterclockwise. The LBFZ is mainly characterized by left-lateral strike-slip and normal faults (SSBRG, 1988; Sun and Deng, 1994; Zhang et al., 1998; Yuan et al., 2004; Liu et al., 2006; Zhang et al., 2006; Wang et al., 2014; Shi et al., 2015; Zheng et al., 2016; Wang, S.D. et al., 2018).

The LQF is a left-lateral strike-slip fault. It is a marginal fault on the southwest margin of the Ordos block and has been active since the late Pleistocene (SSBRG, 1988; Lin et al., 2015; Zheng

et al., 2016; Li, X.N. et al., 2018). It is the largest and most active fault in the LBFZ, with an average left-lateral slip rate of 0.5–0.9 mm/yr (Lin et al., 2015; Li, X.N. et al., 2018; Wang et al., 2021). On the northeast side of the fault, the lithology is mainly Mesozoic clastic sedimentary rocks (e.g., sandstone and conglomerate) and Quaternary loess. On the southwest side of the fault, the lithology is mainly Quaternary loess (Fig. 2a). The LQF can be identified from the linear tectonic and geomorphological features in satellite images.

The TGF is the west boundary of the LBFZ. It extends for about 75 km and is inactive in the late Quaternary (SSBRG, 1988). The west side of the TGF is dominated by pre-Cretaceous metamorphic rocks (marble and gneiss) and granites, while the east side is dominated by Cretaceous sedimentary rocks (conglomerate and sandstone) and Quaternary loess (Bureau of Geology and Mineral Resources of Shaanxi Province, 1989; Li, X.N. et al., 2018; Liu et al., 2020).

The GGF and the QBF are the west and east boundaries of the Qianyangling Uplift, which is composed of Ordovician limestone (Fig. 2a). The GGF extends for about 70 km. It is active in the Late Quaternary and has clear geomorphic scarps (Shi et al., 2015; Zhang et al., 2017). The QBF is inactive in the Quaternary because there is no clear activity on the Quaternary loess platform (Li et al., 2019).

3. MATERIAL AND METHODS

We used ArcGIS10.2 to extract data of the Qianhe, Hengshuihe, and Jinlinghe River Basins (Fig. 2b) from the Advanced Spaceborne Thermal Emission and Reflection Radiometer Global Digital Elevation Model (ASTER GDEM), which has a spatial resolution of 30 m. We evaluated the tectonic activity of the study area by analyzing different geomorphic indices; these include the hypsometric integral (HI) and hypsometric curve, standardized stream length-gradient index (SL/K) and Hack profile, elongation ratio (Re), drainage basin asymmetry factor (AF), and valley floor width-to-height ratio (VF).

3.1. Hypsometric Integral (HI) and Hypsometric Curve

The hypsometric curve was proposed by Strahler (1952) based on the Davis tectonic cycle theory, which uses the relative area ratio and relative height ratio as the horizontal and vertical axes, respectively. The hypsometric curve reflects the relationship between the horizontal cross-sectional area of a plane in a drainage basin and the elevation of that plane relative to the watershed outlet. It is a geomorphic index that describes the volumetric residual rate of the surface in three-dimensions with a two-dimensional curve structure.

The HI index is the area below the hypsometric curve and reflects the relative volume of the drainage basin that has not been eroded. It is defined as the elevation distribution of a given area of the drainage basin. The HI index is very sensitive to the level of tectonic activity and is a powerful tool to distinguish between tectonically active and inactive areas (Strahler, 1952; Schumm, 1956; Pike and Wilson, 1971; Mayer, 1990; Keller and Pinter, 2002). Pike and Wilson (1971) concluded that the elevation relief ratio is approximately equal to the HI value, so a simple calculation formula for the HI was derived as follows:

$$HI = (H_{mean} - H_{min})/(H_{max} - H_{min}), \quad (1)$$

where H_{max}, H_{min}, and H_{mean} are the highest, lowest, and average elevations in the area, respectively. Its value varies between 0 and 1. According to Davis' cycle of erosion (Davis, 1899), when the landform development is in the early stage, its tectonic activity is strong, erosion is weak, and the high elevation area is dominant, so it should have a higher HI value, and the hypsometric curve is convex. At the old stage of landform development, the area is tectonically inactive, erosion is high, slopes are gentle, so it has a lower HI value, and the hypsometric curve is concave. In areas with moderate tectonic activity, the hypsometric curve is S-shaped (Lifton and Chase, 1992; Ohmori, 1993; Chen et al., 2003; Liu, 2017; Cheng et al., 2018).

The magnitude of the HI value and the shape of the hypsometric curve is affected by different factors such as tectonics, erosion, lithology, and climate. They can be used to identify the development stage and tectonic activity level of a basin (Ohmori, 1993; Weissel et al., 1994; Willgoose and Hancock, 1998; Brocklehurst and Whipple, 2004; Cheng et al., 2012; Xu et al., 2013; Faghih et al., 2016; Su et al., 2016; Shi et al., 2019; Guan et al., 2021). The hypsometric curve was acquired using CalHypso Tools, an ArcGIS add-in developed by Pérez-Peña et al. (2009a).

3.2. Standardized Stream Length-Gradient Index (SL/K) and Hack Profile

In a river system, a dynamic equilibrium is reached when the erosion is equal to the uplift. Thus, the river system tends to form a concave longitudinal profile under natural evolution (Schumm et al., 1956; Hack, 1973). This stable profile of the river system tends to deviate due to the influence of various factors, mainly lithology, climate, or tectonic. To quantitatively analyze the variation of river gradient, Hack (1973) proposed the stream length-gradient index (SL). The SL index is defined as:

$$SL = (\Delta H/\Delta L) \times L, \quad (2)$$

https://doi.org/10.1007/s12303-023-0023-8

where ΔH is the difference between the highest and lowest points of each river section, ΔL is the length of the river section, and L is the channel length from the source of the river to the midpoint of the river section. The SL index can be used to assess the impact of environmental variables on rivers and to evaluate whether a river basin has reached a state of equilibrium. It is a powerful tool that is widely used in assessments of tectonic activity based on geomorphic indices (Hack, 1973; Keller and Pinter, 2002; Chen et al., 2003; Pérez-Peña et al., 2009b; Dey et al., 2019).

The SL is more sensitive to changes in riverbed slope because even small changes in the slope (ΔH/ΔL) of the river section, are enhanced through its product with the channel length (L). For a basin that is in a state of equilibrium, its SL value will remain constant (Hack, 1973), while local tectonic activity or lithologic differences lead to abrupt changes in SL values. A high SL value is often related to high riverbed erosion resistance, or the river section being in a tectonic uplift area. A low SL value is related to low riverbed erosion resistance, tectonic inactivity area, or when streams flow through strike-slip faults (Brookfield, 1998; Keller and Pinter, 2002; Chen et al., 2003; Troiani and Della Seta, 2008; Dehbozorgi et al., 2010; Zhao et al., 2014; Graveleau et al., 2015; Ntokos et al., 2016; Yang, Y. et al., 2022).

The Hack profile is a longitudinal profile of the river section; its vertical axis is elevation and its horizontal axis is the logarithm of the river section length. A convex profile indicates high tectonic activity. A concave profile or a profile with a straight line indicates low tectonic activity (Hack, 1973; Zhao et al., 2010; Zhang et al., 2018). The graded river gradient (K) is the slope of the line from the source to the mouth of the river on a Hack profile. Since the SL value is greatly influenced by the channel length, to compare the SL values of different rivers, it is necessary to standardize the SL index by K and obtain the SL/K index (Seeber and Gornitz, 1983; Chen et al., 2003; Pérez-Peña et al., 2009b; Wu et al., 2014, Zhao et al., 2014). We used the index of SL/K, and the K is defined as:

$$K = H_{total}/LnL_{total}, \quad (3)$$

where H_{total} and L_{total} are the altitude difference and the length of the whole channel, respectively. The SL/K index is highly sensitive to changes in channel slope (Chen et al., 2003; Troiani and Della Seta, 2008; Pedrera et al., 2009). If there is little change in climate and lithology, high SL/K is usually associated with a high uplift rate, and an abnormally high SL/K value usually corresponds to the presence of knickpoints. The index is widely used to detect active tectonics and uplift (Monteiro et al., 2010; Gao et al., 2013).

3.3. Elongation Ratio (Re)

Elongated drainage basins are topographic features that are actively rising, while circular basins are the results of basin development with divide migration and stream capture (Bull, 2009). Thus, elongated and circular basins indicate tectonically active and inactive areas, respectively (Canon, 1976; Ramirez-Herrera, 1998; Figueiredo et al., 2019). The shape of a drainage basin can be described by Re, which is a dimensionless quantity that can be used to compare the level of tectonic activity of different drainage basins (Rimando and Schoenbohm, 2020). It is an important geomorphic index that supports the neotectonic activity of a watershed (Gupta et al., 2022). For a given drainage basin, Re is defined as the ratio between the diameter of a circle with the same area as the basin and the maximum length of the basin (Schumm, 1956):

$$Re = 2 \times (\sqrt{A}/\pi)/L_b, \quad (4)$$

where A is the area of the basin, and L_b is the distance between the mouth of the river and the most distant point in the basin. Values of Re vary between 0 and 1, and are generally between 0.6 and 1.0 for various climate and geological conditions (Strahler, 1964). When the Re value is close to 1, the shape of the basin tends to be circular, indicating a low relief and flat slopes in the area, and also represents a stable state of tectonic activity; while as the Re value decreases, the shape of the basin shows an elongated shape, usually characterized by high relief and steep slopes with high relative uplift, and also indicates tectonic activity (Strahler, 1964; Regard et al., 2009; Rimando and Schoenbohm, 2020). Values of < 0.50, 0.50–0.75, and > 0.75 indicate basins that are tectonically active, slightly active, and inactive (stable), respectively (Bull and McFadden, 1977; Cuong and Zuchiewicz, 2001).

3.4. Drainage Basin Asymmetry Factor (AF)

Proposed by Hare and Gardner (1985), the AF is a quantitative morphometric method that describes the pattern and geometry of the stream network within a catchment. It is defined as:

$$AF = (A_r/A_t) \times 100, \quad (5)$$

where A_r is the area of the basin to the right (facing downstream) in the direction of stream flow, and A_t is the total area of the drainage basin. The migration of a river channel perpendicular to its axis may occur because of internal processes in the river or tectonic tilting of the ground surface, so the AF is sensitive to changes in lithology or tectonic tilt perpendicular to the channel (El Hamdouni et al., 2008). It can be used to evaluate the tectonic tilt of the drainage basin or larger areas, in response to tectonic activity or lithologic control (Hare and Gardner, 1985; Gardner et al., 1987; Cox, 1994; Keller and Pinter, 2002; Tsodoulos et al., 2008; Giano et al., 2018).

The AF values close to 50 indicate little or no tectonic activity and very little or no tilt perpendicular to the direction of the channel (Hare and Gardner, 1985). Under the influence of tectonic activity or lithologic control, values gradually deviate from 50; tilt perpendicular to the channel and basin asymmetry increase (Giano et al., 2018). Values of > 50 and < 50 are associated with the basin tilting to the left and to the right, respectively (Keller and Pinter, 2002). For cases with the same lithologic conditions, AF values can be used to determine differences in tectonic activity level. Following El Hamdouni et al. (2008) and Pérez-Peña et al. (2010), we used |AF–50| to quantify the symmetry of the drainage basin. Values of |AF–50| were categorized into three classes. Values of > 15, 7–15, and < 7 correspond to classes 1 (high), 2 (moderate), and 3 (low) in basin asymmetry, respectively.

3.5. Valley Floor Width-to-Height Ratio (VF)

The VF was originally developed to assess changes in erosional patterns and drainage response to base level changes in mountain fronts, and through it to assess their relative activity or tectonic base level fall (Bull and McFadden, 1977; Rockwell et al., 1985; Silva et al., 2003). This geomorphic index can distinguish between V-shaped valleys formed by active uplift and U-shaped flat wide valleys formed by lateral erosion in response to the base level of stability (Bull and McFadden, 1977; Bull, 1978; Dumka et al., 2019). The VF is the ratio of the valley floor width to its average height and is defined as:

$$VF = 2V_{fw}/[(E_{ld} - E_{sc}) + (E_{rd} - E_{sc})], \quad (6)$$

where V_{fw} is the width of the valley floor, E_{sc} is the elevation of the valley floor, E_{ld} and E_{rd} are the elevations of the left and right (facing downstream) valley shoulders, respectively. The value of VF is very sensitive to tectonic uplift. It indicates the degree of valley floor erosion and tectonic activity. Smaller VF values correspond to narrow V-shaped valleys, which are characteristic of active river downcutting and are usually associated with rapid uplift in a tectonically active setting. In contrast, higher VF values correspond to wide, flat U-shaped valleys, indicating that degradation and denudation processes, such as valley widening and ridge-crest lowering, dominate the recent landscape and are typically associated with tectonically stable settings (Bull and McFadden, 1977; Rockwell et al., 1985; Keller, 1986; Keller and Pinter, 2002; Silva et al., 2003; Bull, 2007; Seong et al., 2008; Burbank and Anderson, 2012; Figueiredo et al., 2019).

River valley morphology can be affected by lithology, and the shape of the river valley may vary along the length of the river (Ramírez-Herrera, 1998). Therefore, we calculated the VF value at 1–3 km from the estuary for each channel to facilitate comparison between channels in different catchments (Silva et al., 2003; Bull, 2007; Mahmood and Gloaguen, 2012). For larger drainage basins, we used the average VF value from multiple profiles.

4. RESULTS

4.1. HI

Values of HI in the Qianhe, Hengshuihe, and Jinlinghe River Basins are 0.1174–0.6860, 0.1429–0.8479, and 0.2665–0.4895, respectively. Following El Hamdouni et al. (2008), we categorized HI values into three classes. Values of > 0.5, 0.3–0.5, and < 0.3 correspond to classes 1 (high), 2 (moderate), and 3 (low) in tectonic activity. Figure 3a shows that the HI values in the LBFZ are generally high, and most values are in classes 1 and 2. In the Qianhe River Basin, high HI values are found on the east and west sides of the basin. In the Hengshuihe River Basin, high HI values are found on the north and south sides of the basin. The locations of high HI values are mainly located on the LQF and the TGF. Most hypsometric curves are S-shaped and concave; a few curves are convex (Fig. 4). Curve shapes generally correspond to HI values. Because variations in the basin area may affect the magnitude of HI values (Hurtrez et al., 1999), we plotted the relationship between basin area and HI value (Fig. 3b, c). The results show that there is a weak correlation ($R^2 = 0.0445$) between the two variables.

4.2. SL/K and Hack Profile

We calculated SL/K values for the Qianhe, Hengshuihe, and Jinlinghe River Basins at 1500, 1000, and 500 m along the river sections and calculated basin averages. Following El Hamdouni et al. (2008), we categorized SL/K values into three classes. Values of > 3.7, 2.5–3.7, and < 2.5 correspond to classes 1 (high), 2 (moderate), and 3 (low) in tectonic activity. Most SL/K values are in class 1 (Fig. 5a). Basin averages are generally high and are in classes 1 and 2 (Fig. 5b). Average SL/K values for the Qianhe, Hengshuihe, and Jinlinghe River Basins are 0–5.7435, 0–6.4903, and 0–4.6139. The sub-catchments with class 1 SL/K values are concentrated around faults, especially around the LQF and the TGF.

From the Hack profiles of the main tributaries in the area (Fig. 6), we found SL/K values of < 2 in all upstream sections. Abnormally high SL/K values in the middle and lower sections indicate the presence of knickpoints. The Hack profiles of all rivers are generally convex upward, indicating relatively high levels of current tectonic activity. The degree of upward convexity varies and profiles of some tributary sections are concave downward.

https://doi.org/10.1007/s12303-023-0023-8

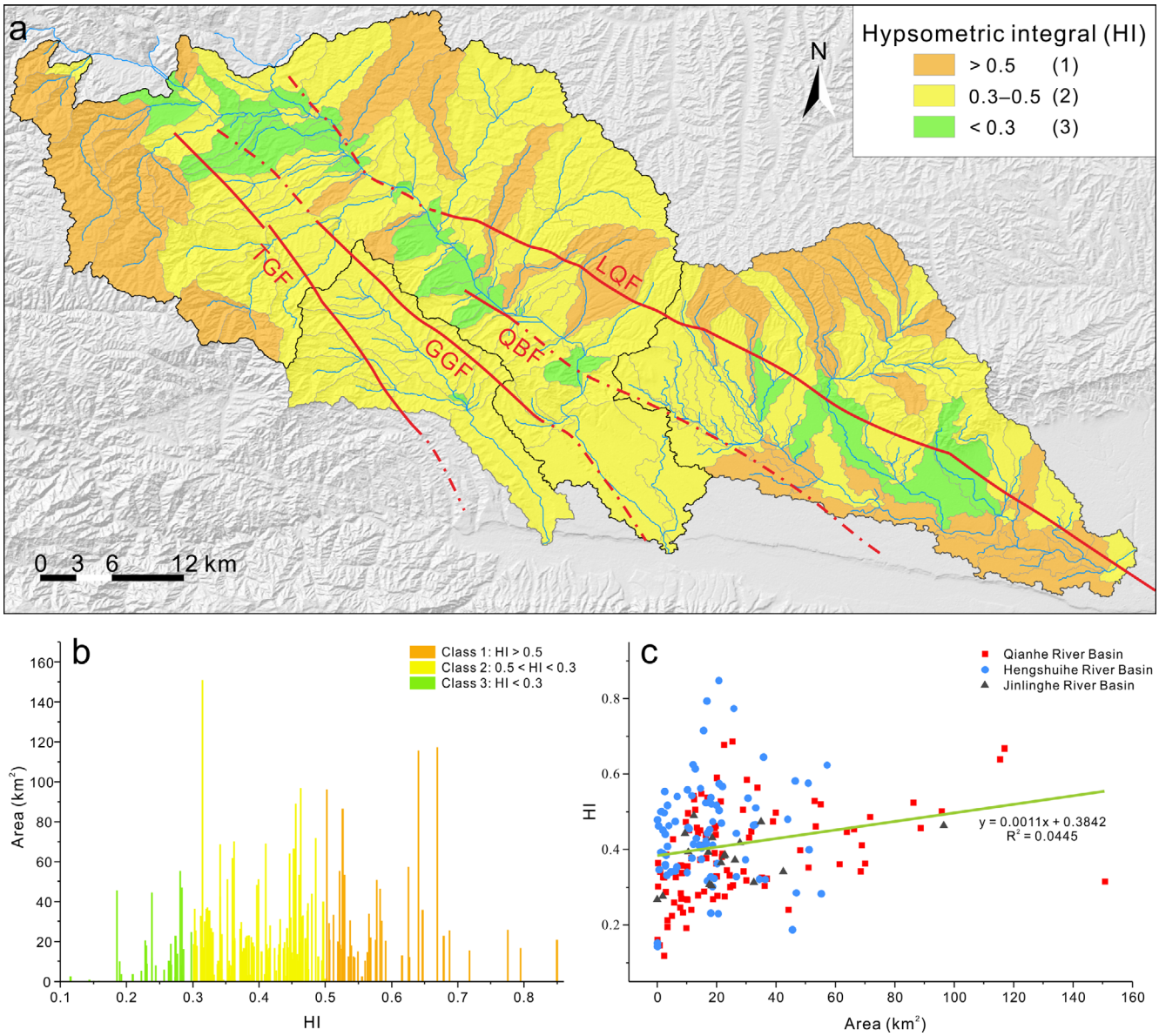

Fig. 3. (a) Distribution map of HI classification. (b and c) The relationship between the basin area and HI. Among them, (b) is a two-dimensional distribution diagram of HI and drainage area; (c) is a scatter diagram of drainage area and HI.

4.3. Re

Values of Re in the Qianhe, Hengshuihe, and Jinlinghe River Basins are 0.2689–0.8438, 0.2167–0.7763, and 0.3784–0.7540, respectively. Figure 7a shows that most Re values are in classes 1 and 2. Class 1 values are concentrated on the north side of Fengxiang District, around Qianyang County, and Longxian County. The few class 3 values are distributed sparsely throughout the study area. Tectonic activity is moderate in the Qianhe River Basin; 28 and 64 sub-catchments have class 1 and 2 Re values, respectively. With 34 sub-catchments with class 1 Re values, tectonic activity is high in the Hengshuihe River Basin. With 12 sub-catchments with class 2 Re values, tectonic activity is moderate in the Jinlinghe River Basin.

4.4. AF

In the Qianhe River Basin, |AF–50| values are 0.4833–40.7407, with more than half of the sub-catchments tilting to the right (facing downstream) (Fig. 8b). In the Hengshuihe River Basin, |AF–50| values are 0.2087–38.9958, with most sub-catchments tilting to the right (facing downstream) (Fig. 8b). In the Jinlinghe River Basin, |AF–50| values are 0.6628–24.3272, with most sub-catchments tilting to the right (facing downstream). Figure 8a shows that AF values are distributed sparsely throughout the study area. High AF values are found in west and southeast

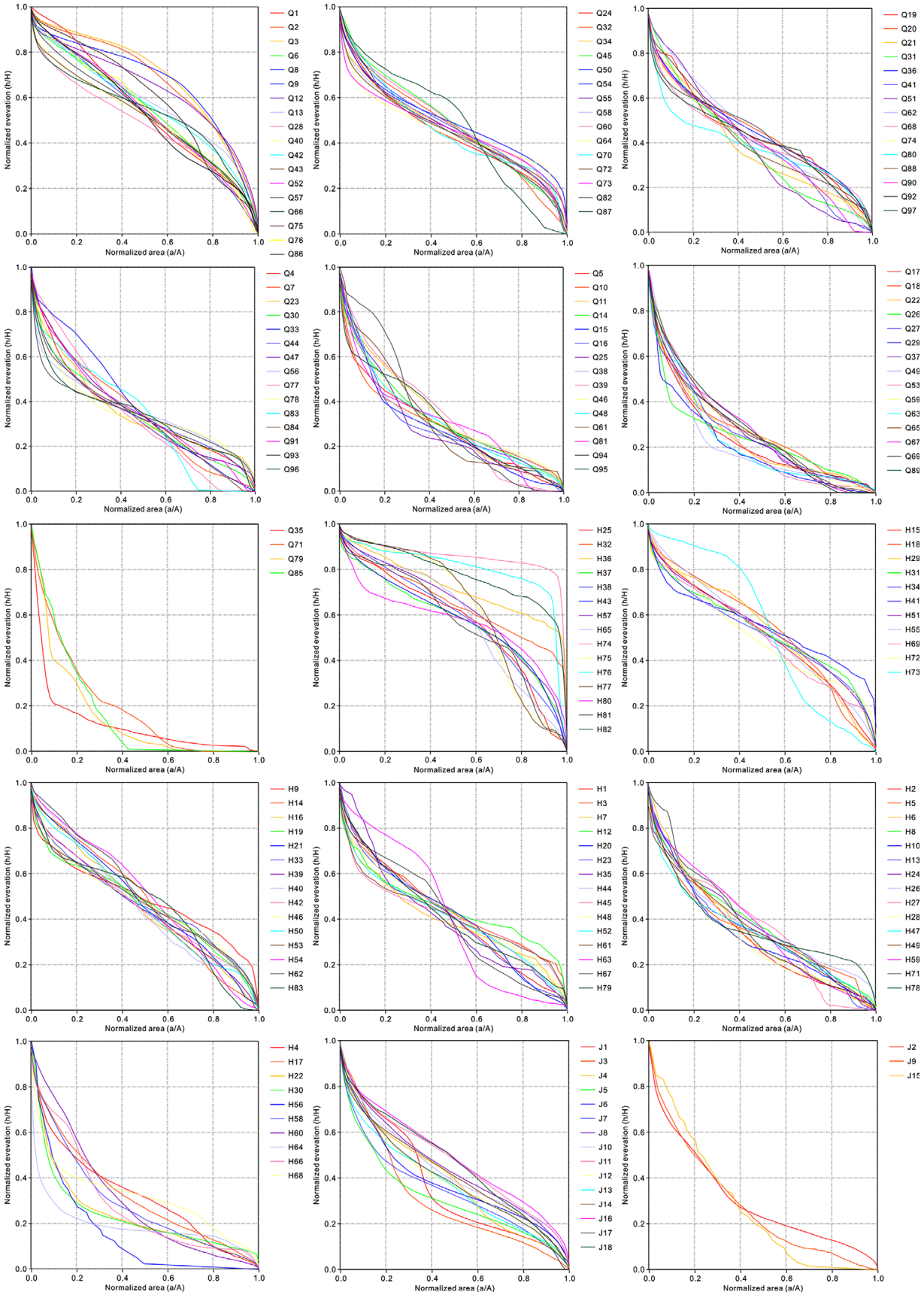

Fig. 4. The hypsometric curves of drainage basins extracted from DEM (see Fig. 2b for the distribution), arranged in the order of Qianhe River Basin, Hengshuihe River Basin, and Jinlinghe River Basin, and plotted from high to low HI values.

https://doi.org/10.1007/s12303-023-0023-8

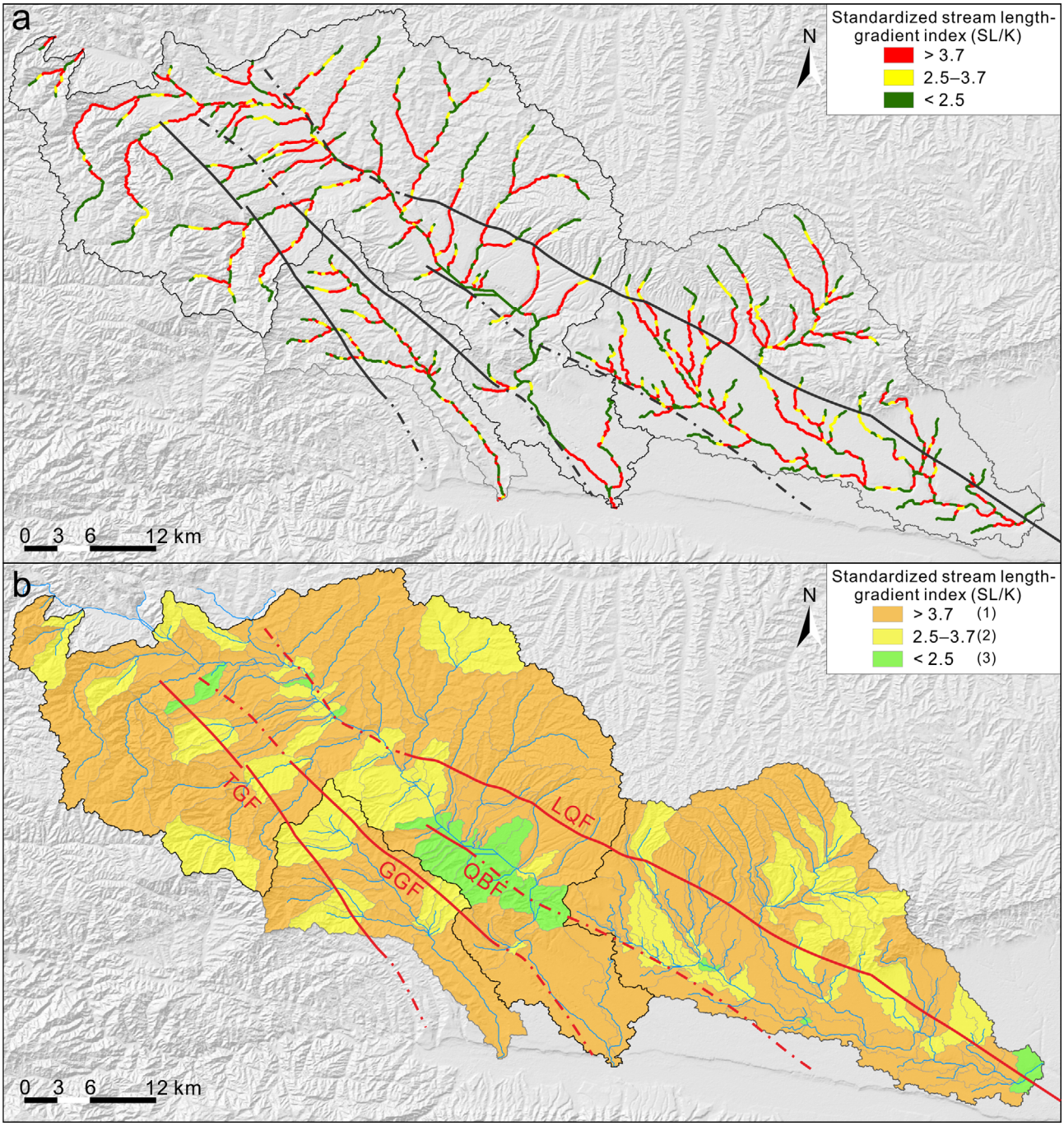

Fig. 5. (a) Distribution map of SL/K value and (b) classification.

Qianyang County, and around Longxian County and Qishan County; asymmetry is high and most sub-catchments with high AF values tilt to the right (facing downstream).

4.5. VF

Values of VF in the Qianhe, Hengshuihe, and Jinlinghe River Basins are 0.0702–48.3283, 0.2532–70.8286, and 0.4547–3.4805, respectively. We categorized VF values into three classes. Values of < 0.5, 0.5–1, and > 1 correspond to classes 1 (high), 2 (moderate), and 3 (low) in uplift rate. Figure 7b shows that high VF values are concentrated on the northeast side of the LQF and the southwest side of the TGF; valleys are V-shaped and VF values are in classes 1 and 2. However, most of the sub-catchments in the south part of the Hengshuihe River Basin are in class 3, and the valleys are U-shaped.

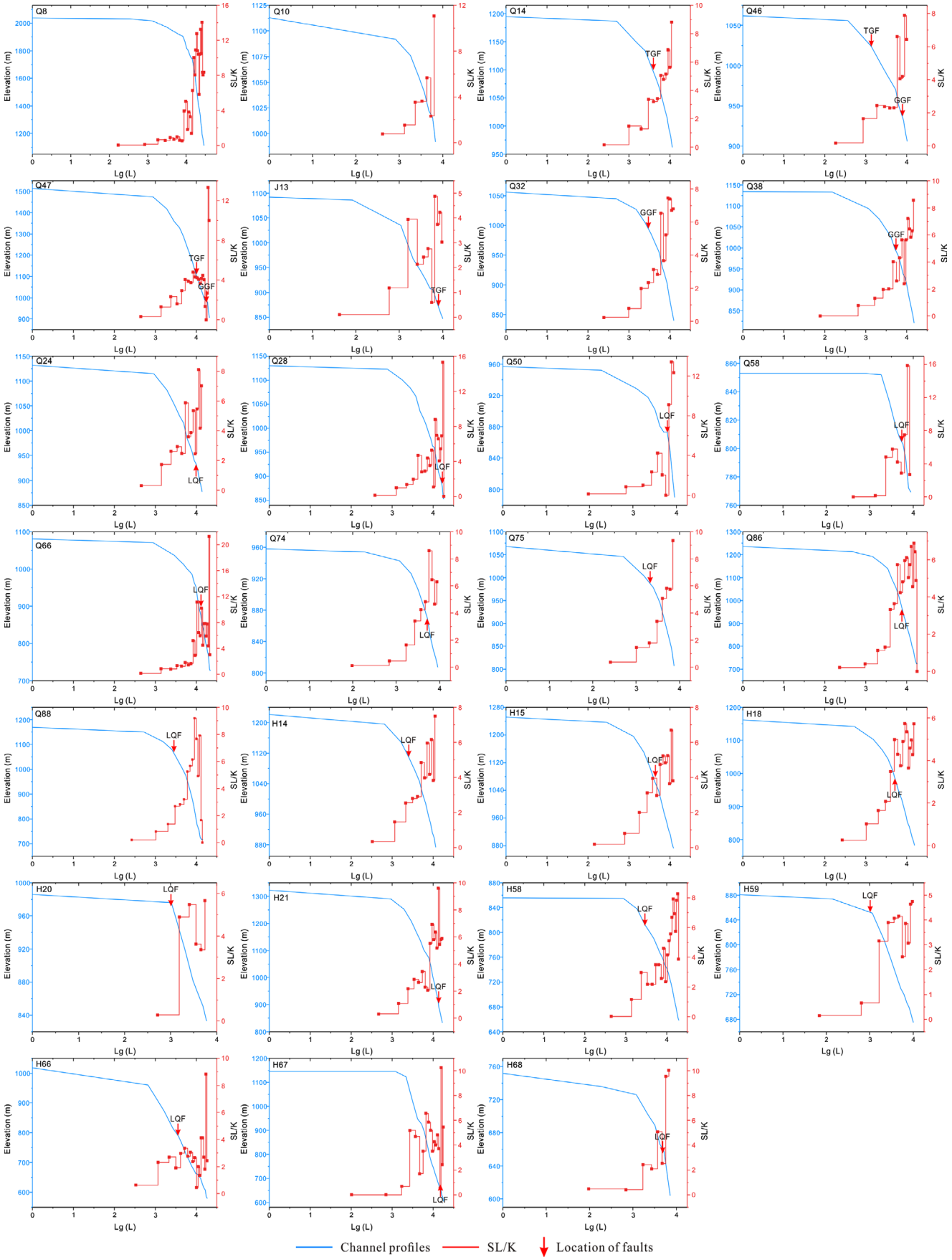

Fig. 6. Standardized stream length-gradient index (SL/K) and Hack profiles of major tributaries.

https://doi.org/10.1007/s12303-023-0023-8

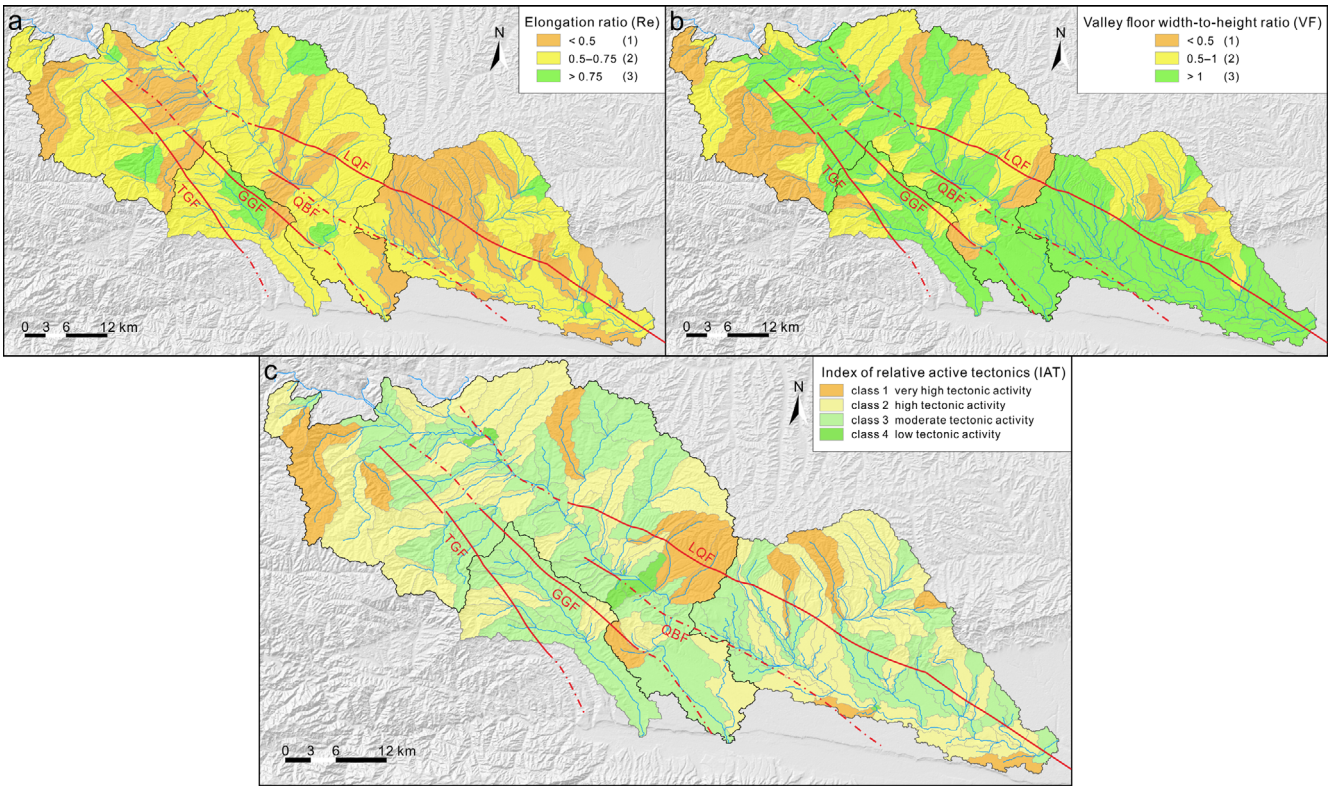

Fig. 7. Distribution of numerical classes of 2 geomorphic indices for drainage basins, and relative tectonic activity classes map. (a) Re. (b) VF. (c) Relative tectonic activity classes (IAT).

5. INDEX OF RELATIVE ACTIVE TECTONICS (IAT)

We analyzed the five geomorphic indices—HI, SL/K, Re, AF, and VF—to evaluate the relative tectonic activity level within the LBFZ. However, index boundary values may vary because of lithologic and structural differences (Rockwell et al., 1985; Wells et al., 1988; Silva et al., 2003; Cheng et al., 2018; Shi et al., 2020). Therefore, we used the IAT proposed by El Hamdouni et al. (2008) to assess the relative tectonic activity in the study area. The IAT is a comprehensive geomorphic index and is defined as IAT = S/n, where S is the sum of the classes of the geomorphic indices of the drainage basin, and n is the number of indices.

The IAT is an effective tool for identifying tectonically active areas and has been widely used in recent years (El Hamdouni et al., 2008; Dehbozorgi et al., 2010; Mahmood and Gloaguen, 2012; Chang et al., 2014; Cheng et al., 2016; Kothyari et al., 2016; Cheng et al., 2018; Shi et al., 2020; Kumar et al., 2022). Values of IAT are obtained by synthesizing the values of various geomorphic indices. We categorized IAT values into four classes (El Hamdouni et al., 2008). Values of < 1.5, 1.5–2.0, 2.0–2.5, and ≥ 2.5 correspond to classes 1 (very high), 2 (high), 3 (moderate), and 4 (low) in tectonic activity, respectively.

In the study area, IAT values are 1.2–2.6, with a mean of 1.95 and a standard deviation of 0.30. Among the 198 sub-catchments in the three major drainage basins, 44.95% or 89 sub-catchments are in classes 1 (13 sub-catchments) and 2 (76 sub-catchments), 52.02% or 103 sub-catchments are in class 3, and 3.03% or 6 sub-catchments are in class 4. This shows that the overall tectonic activity in the LBFZ is relatively high (Fig. 7c). Tectonic activity is relatively high in almost half of the study area. Class 1 values indicate very high tectonic activity and are mostly found along the LQF and the TGF.

6. DISCUSSION

Geomorphic indices are a powerful tool for the quantitative analysis of regional tectonic activity. We analyzed, evaluated, and compared the tectonic activity level of Qianhe, Hengshuihe, and Jinlinghe River Basins using geomorphic indices (HI, SL/K, Re, AF, and VF) and IAT.

6.1. Influencing Factors of Geomorphic Indices

Climate and lithology are important factors affecting geomorphological evolution. When evaluating tectonic activity, the influence of these factors on geomorphic indicators needs to be considered (Keller and Pinter, 2002).

Temporal and spatial variations in Climatic factors, particularly

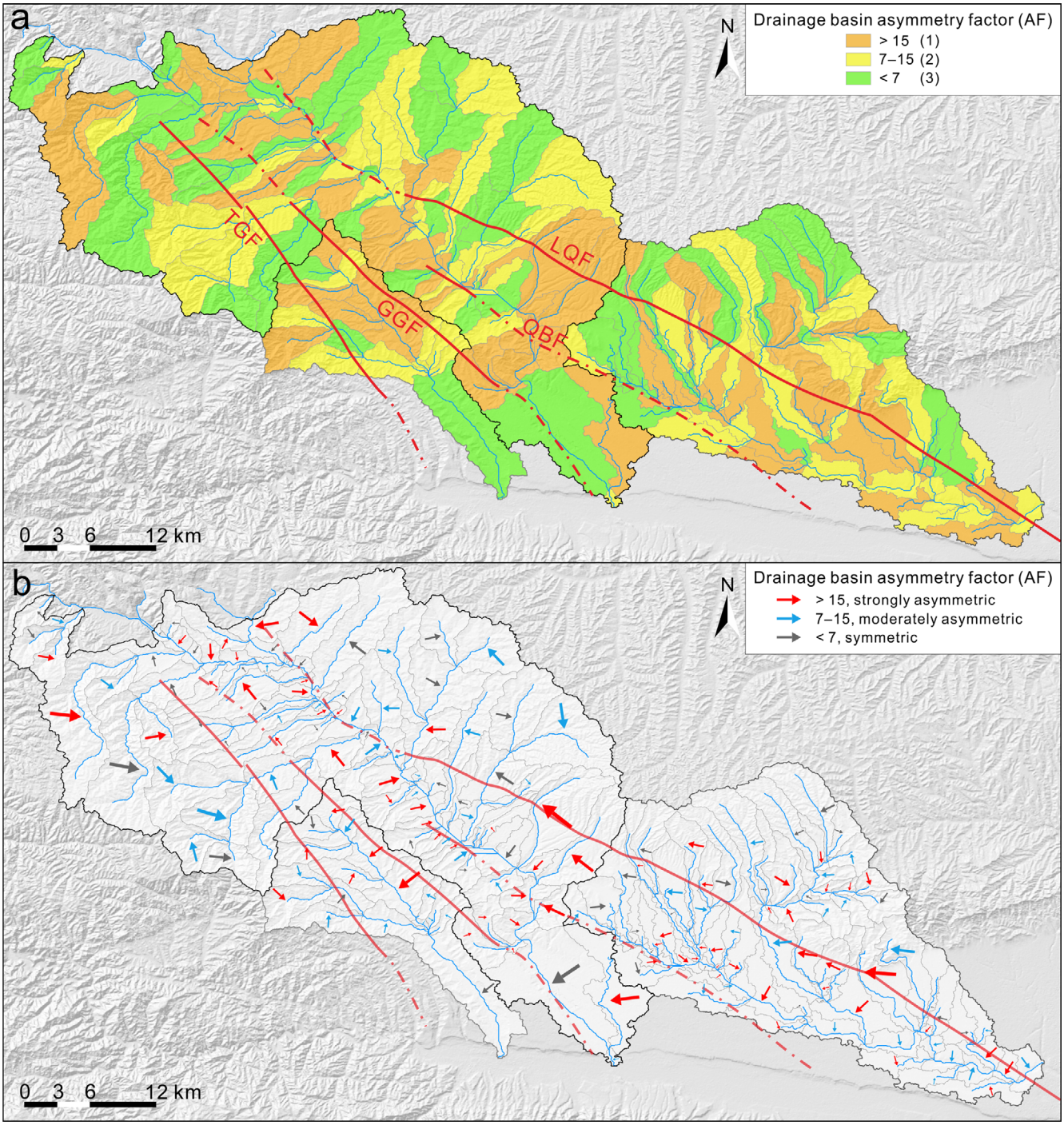

Fig. 8. (a) Distribution map of AF classification. (b) Asymmetry map for drainage basins, the asymmetry direction is indicated by arrows.

precipitation, may have a significant impact on geomorphic indices (Kirby and Whipple, 2012). According to the distribution of annual average precipitation in the study area (Fig. 9), the overall variation of precipitation in the watersheds within the area is small, and the climatic conditions are basically the same. At the same time, the distribution is characterized by low values in the north and high values in the south, with the low values of precipitation mainly concentrated in Longxian and Qianyang counties and the high values mainly concentrated in Baoji urban area and Guozhen town. After comparison, it was found that the spatial distribution of the values of various geomorphic indices did not show a tendency to change along with precipitation. Therefore, the influence of precipitation on the geomorphic indices in the study area is not significant, and the influence of precipitation can be excluded.

The influence of lithology on geomorphic indices cannot be

https://doi.org/10.1007/s12303-023-0023-8

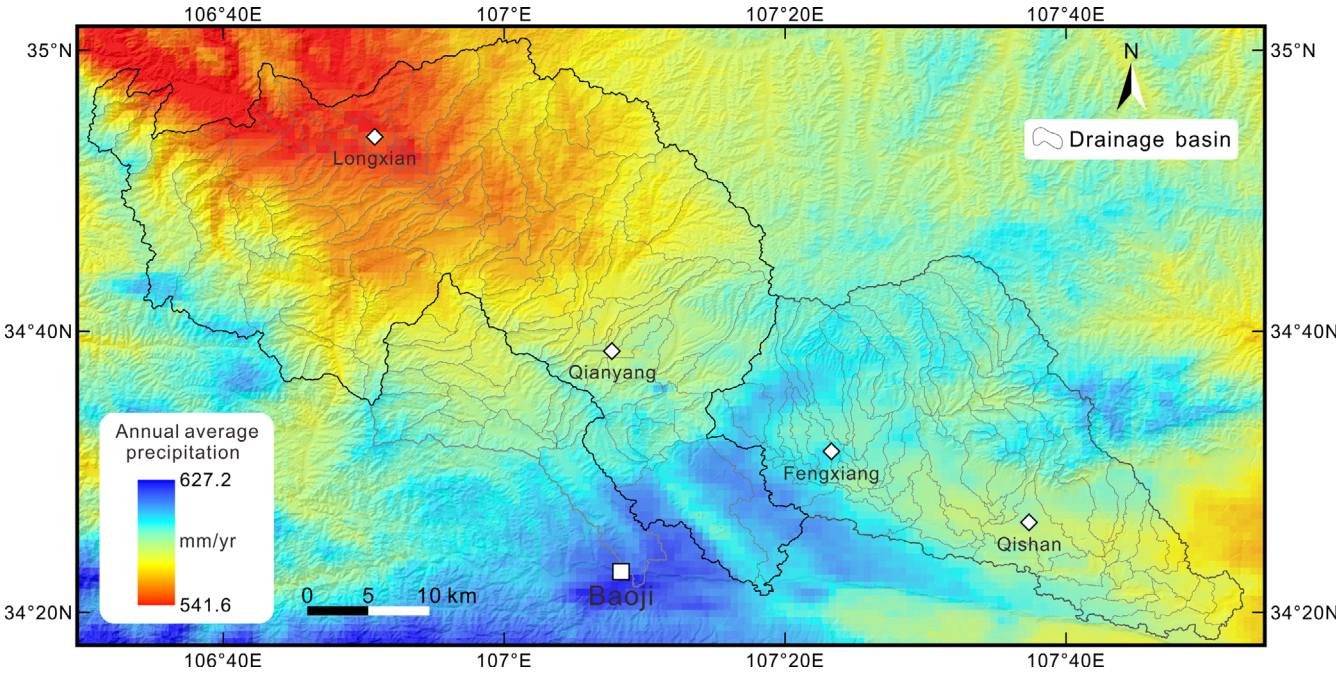

Fig. 9. Map of average annual precipitation in the study area. The data used are 1 km resolution annual precipitation data (2001–2020) of China from the National Earth System Science Data Center, National Science & Technology Infrastructure of China (http://www.geodata.cn).

ignored. In small catchments, the HI values are mainly affected by lithologic factors, while in larger catchments, the HI values are more significantly affected by tectonic factors (Lifton and Chase, 1992; Hurtrez et al., 1999; Chen et al., 2003; Zhang et al., 2015). In addition, the SL values may also change when rivers flow through rock units with different resistance to erosion (Hack, 1973). Comparing the spatial distribution of HI and SLK values with the geologic map, it is found that high HI values not only exist in the rock units (granite, amphibolite, marble, and gneiss) with strong erosion resistance in the Longxi block but also found in Mesozoic clastic sediments (sandstone, conglomerate, shale, and mudstone) with weaker erosion resistance and Cenozoic sediments (clay and loess) with even weaker erosion resistance, such as Q28, Q57, Q86, H18, H36, H43, H74, and other sub-catchments. At the same time, some rock units with high erosion resistance do not have higher HI values than those with weak erosion resistance; SLK values even show high values across the region. From these comparisons, we conclude that the influence of lithology on the geomorphic indices of the study area is limited.

In summary, the observed variation of geomorphic indices in the area is mainly related to tectonic activity, while other factors such as lithology and climate have a limited influence on these indices and can be excluded from consideration. Therefore, the spatial distribution of the values of the indices in the Qianhe, Hengshuihe, and Jinlinghe River Basins provides a basis for understanding Quaternary tectonic activity in the area. The tectonic activity and relative uplift of the LBFZ gave rise to a range of geomorphological responses, manifested by rivers with generally high SL/K values, drainage basins with relatively high HI and low Re values, basins with different degrees of asymmetry, and leading edges of mountains with low VF values.

6.2. Geomorphic Indices Analysis

The three major drainage basins are elongated with class 1 and 2 Re values (Fig. 7a); this indicates high tectonic activity, which is concentrated on the northwest side of the Hengshuihe River Basin. Similar results were obtained for HI and SL/K values (Figs. 3a and 5). Higher HI values indicate relatively young fault-related features and higher SL/K values indicate higher uplift and erosion rates. Among the different Hack profiles (Fig. 6), the profile of the river flowing through the LQF and the TGF has the highest convexity, this indicates large differential uplift of the LQF and the TGF. The abnormally high SL/K values correspond to the faults within the drainage basin, which are located very close together. In terms of tectonic tilt, AF values show regional zoning on both sides of the fault zone (Fig. 8b). On the TGF and its southwest side (Longxi block), the drainage basin shows obvious tilt to the east and southeast. On the LQF and its northeast side (the southwest margin of the Ordos block), the watershed shows a tilt to the west and northwest. These indicate that tectonic activity has influenced the evolution of the watershed in this area. It is worth noting that on the LQF, the

basin tilts mostly to the right (facing downstream). Lower VF values around the TGF, LQF, and Qianyangling Uplift indicate higher uplift and cleavage rates (Fig. 7b).

We also found inconsistencies among the indices. On the southeast side of the LQF and TGF, the low upward convexity of the Hack profiles of sub-catchments H66, H68, and J13 indicate relatively low uplift rates in the area (Fig. 6). However, also on the southeast side of the LQF is sub-catchment H67, which is affected by the Northern Weihe Fault and has a Hack profile with relatively high upward convexity (Fig. 6). These characteristics are well present in the distribution of VF values (Fig. 7b), but are not evident in the distribution of SL/K values (Fig. 5b); this indicates a high level of consistency between VF values and Hack profiles. Most of the hypsometric curves of the three major drainage basins are S-shaped and concave (Fig. 4); this indicates that the basins are well into the middle-old stage of evolution. This tendency to stability may be related to the high erosion rate in the area since the Cenozoic, which is controlled by the LBFZ. Hypsometric curves of some sub-catchments in the Qianhe (Q2, Q3, Q8, Q12, Q13, Q42, Q66, and Q75) and the Hengshuihe River Basins (H32, H36, H37, H38, H57, H74, H75, H76, H77, H80, and H82) are convex (Fig. 4). This indicates relatively young basins with little erosion. HI values of them are 0.5276–0.8479 (class 1) and distributed in the west of the TGF, around Qianyang County, and on the north and south sides of the Hengshuihe River Basin. Among all the sub-catchments, those on the south side of the Hengshuihe River Basin (H74, H76, H82, and H36) have the highest HI values and their hypsometric curves have the highest convexity, and they also have high SL/K values (class 1). However, the VF values of them are generally high (class 3), which indicates U-shaped valleys with low tectonic activity (Fig. 7b). This is because these sub-catchments are in the Weihe Graben and the terrain is relatively flat, in line with the definition of the VF index.

The IAT can be used to examine the spatial variations in tectonic activity in areas with relatively high tectonic activity (El Hamdouni et al., 2008; Shi et al., 2020). Values of IAT indicate that the basins with the highest tectonic activity show a distribution along the fault zone (Fig. 7c). They are mostly distributed on the Ordos Block and Longxi Block, which implies that the tectonic activity of the LQF and the TGF are the two strongest in the LBFZ (the LQF and the TGF, as boundary faults, control the geomorphological evolution of the Ordos Block and Longxi Block in the region, respectively). For comparison, we extracted the drainage basins passing through the LQF and TGF based on Figure 7c, and it can be clearly seen that the tectonic activity of the LQF is stronger than that of the TGF (Fig. 10). Among them, the activity of the LQF varies roughly along the strike (from northwest to southeast); it is high on the northwest side, rises to very high along the strike, then

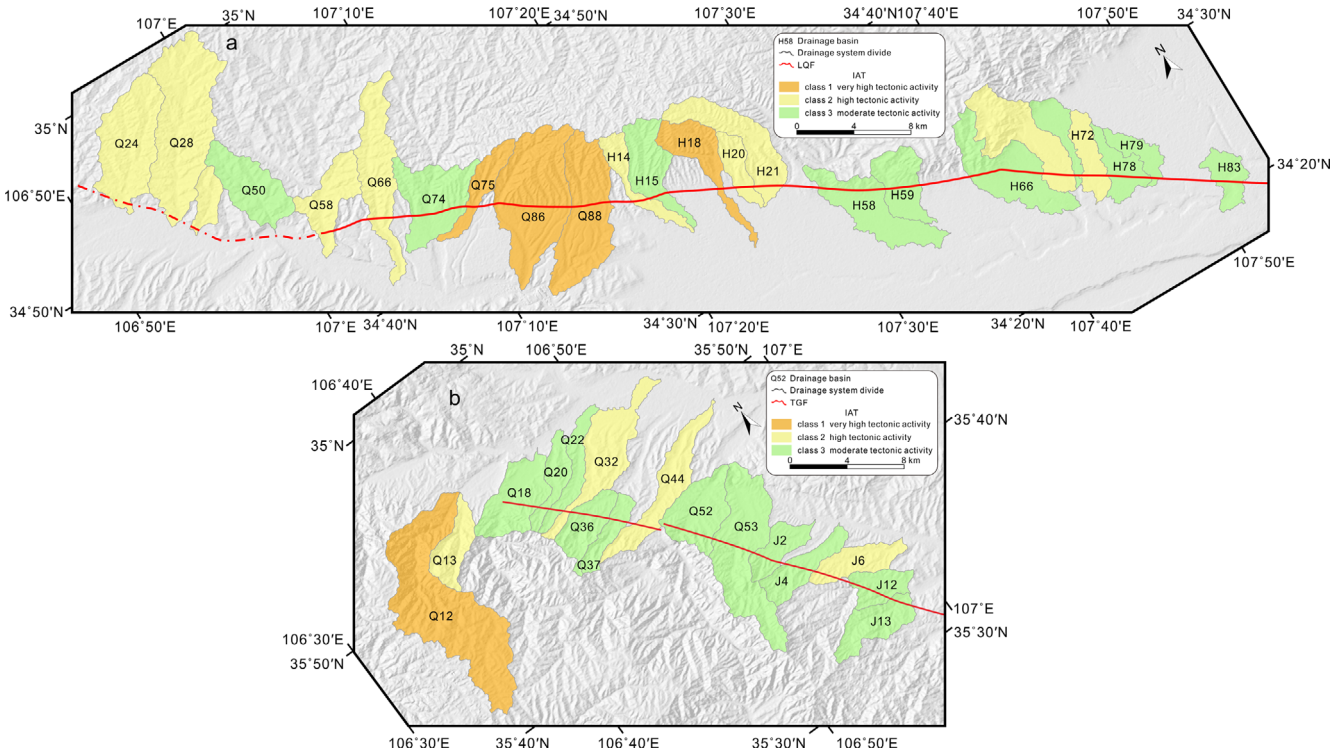

Fig. 10. Comparison of the tectonic activity of the LQF and the TGF. (a) The LQF. (b) TGF. For the LQF, we selected the drainage basins corresponding to its major tributaries for comparison.

https://doi.org/10.1007/s12303-023-0023-8

drops to high and finally medium on the southeast side. The activity of the TGF is high on the northwest side and low on the southeast side. The tectonic activity of the GGF and QBF are the two weakest in the LBFZ, because most of the IAT values of the QBF are in the classes 3 and 4, so the tectonic activity of the GGF is stronger than that of the QBF. Along the strike of the GGF (from northwest to southeast), activity is high on the northwest side, drops to medium along the strike, then rises to very high, and finally drops to medium on the southeast side (Fig. 7c). The activity of the QBF gradually increases along the southeast strike.

6.3. Geomorphology and Tectonic Implications

The results of geomorphic indices indicate relatively high tectonic activity in the study area. Through the IAT, we evaluate

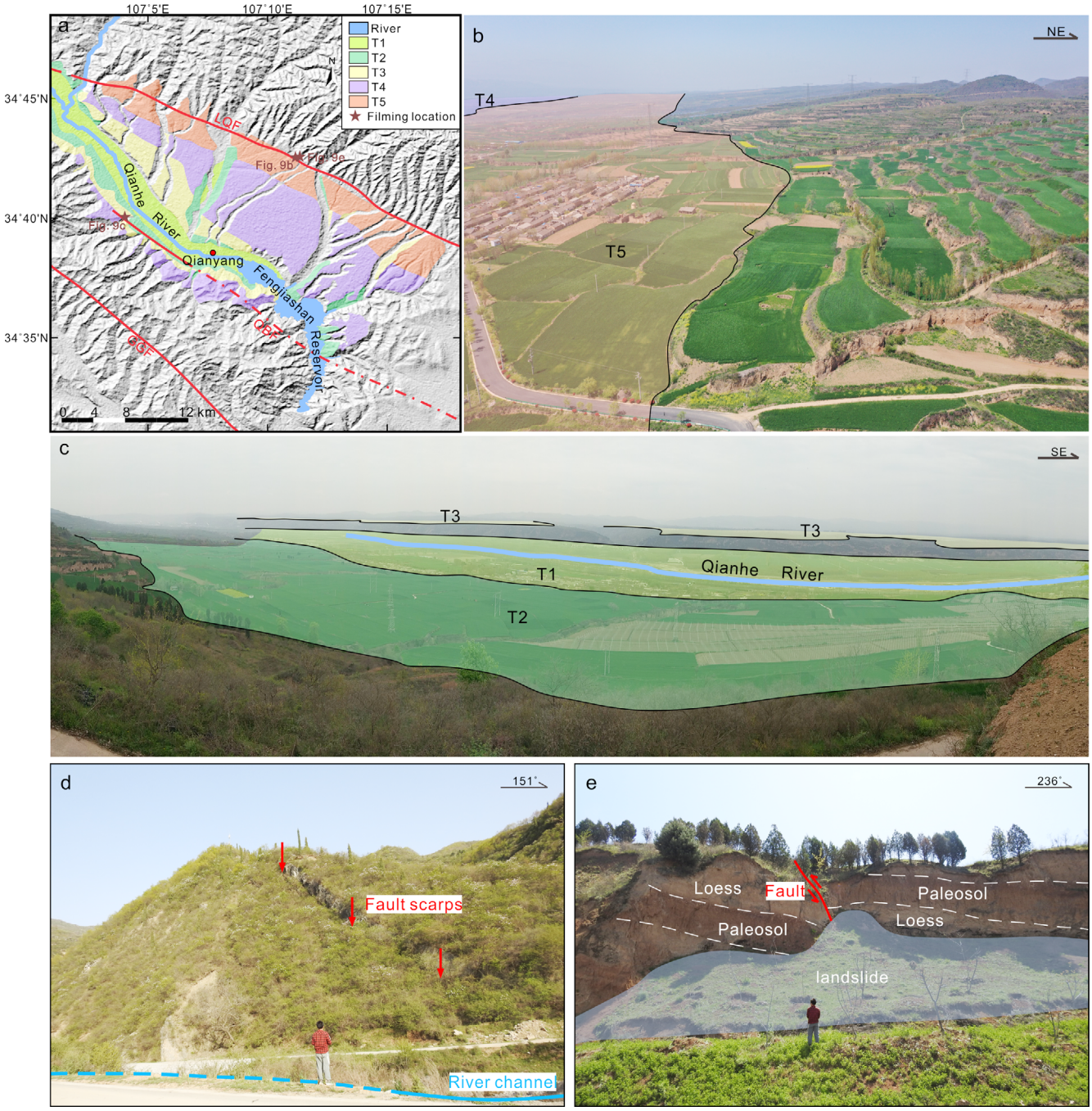

Fig. 11. (a) The five-level terrace of Qianhe River, modified from Chen, S.E. et al. (2018), the asterisks represent the shooting positions of Figure 9b, c. (b) Terrace photo from UAV (Unmanned aerial vehicle). (c) Panoramic photo of terrace taken from a mobile phone. (d) Fault scarps were observed in the field. (e) Field outcrop photographs near the LQF.

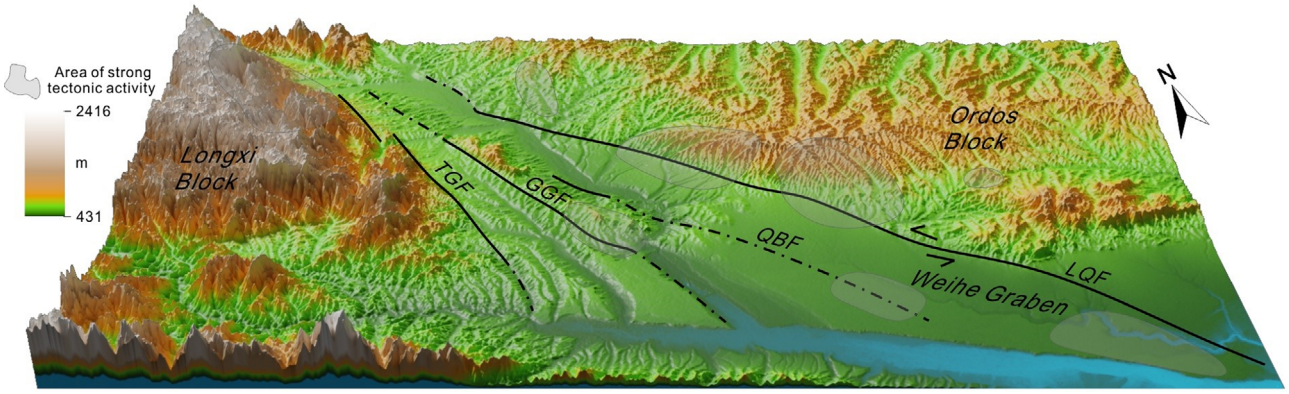

Fig. 12. 3D topographic map of the LBFZ, with the most intense areas of tectonic activity marked on the map.

the relative tectonic activity of the faults within the LBFZ. Previous studies (Zhang et al., 2019; Liu et al., 2020; Li et al., 2022) have shown that topographic changes in the LBFZ are closely related to tectonic activities controlled by faults. The Qianhe River has five terraces (Fig. 11), which indicate Quaternary uplift. Fault scarps (Fig. 11d) and active fault outcrops (Fig. 11e) are also evidence of fault activity. The differences between the elevations of the topographic features on both sides of the LQF and the TGF are the largest in the LBFZ (Fig. 12); this implies substantial uplift and high tectonic activity in the LQF and TGF. Our results are consistent with recent studies (Figs. 7c and 12), which report that the LQF has the highest strike-slip rate and activity in the LBFZ (Li, X.N. et al., 2018; Wang et al., 2021).

The LBFZ is the leading edge of the northeastward expansion of the Tibetan Plateau. The expansion of the Tibetan Plateau was restricted by the Ordos block, which caused its tectonic stress to shift from northeast to southeast (Meyer et al., 1998; Tapponnier et al., 2001; Yuan et al., 2013; Zheng et al., 2013). The Longxi block also shifted from moving northeastward to eastward, and then southeastward (Wang et al., 2013; Lei et al., 2016; Zheng et al., 2016; Wang et al., 2021). The LBFZ absorbed and accommodated the deformation between the Longxi and Ordos Blocks, and the LQF carried out sinistral strike-slip motion in the Early Quaternary (Li, X.N. et al., 2018, 2019; Wang et al., 2021; Li et al., 2022). Our findings are consistent with the results from other studies. Geophysical studies (Tang et al., 2015; Wang, Z.Y. et al., 2018) have shown that the flow of the lower crust of the Tibetan Plateau causes the tectonic deformation within the LBFZ, which is controlled by the northeastward expansion of the Tibetan Plateau. In addition, the crustal horizontal velocity field derived from Global Positioning System and the crustal vertical velocity field derived from precise leveling (Li, Y.H. et al., 2018; Wang and Shen, 2020) indicate southeastward movement in the Longxi block on the west side of the LBFZ and deformation on the southwest margin of the Ordos Block. Cooling history (Yu et al., 2021) shows that the expansion of the Tibetan Plateau has spread to the southwest margin of the Ordos Block. These results suggest that the northeastward expansion of the Tibetan Plateau has affected the LBFZ region. It has caused a near southeastward tilt of the drainage basin in the west part of the LBFZ. Under the influence of the Ordos Block, the northeastward expansion has resulted in the northwestward tilt of the drainage basin in the east part of the LBFZ. Because the tectonic geomorphology of the LBFZ has been considerably affected by the northeastward expansion of the Tibetan Plateau, the drainage pattern and fluvial geomorphology in the study area provide important evidence for the tectonic deformation in the area. We found that the fluvial system responded to the tectonic deformation, and we obtained consistent results from the different geomorphic indices of the LBFZ, such as high HI and SL/K values, elongated basin, deep valleys, and AF values consistent with tectonic stress direction. Our results confirm that the tectonic deformation in the region is controlled by the stress brought about by the northeastward expansion of the Tibetan Plateau.

7. CONCLUSION

We used ASTER GDEM data of three major drainage basins—Qianhe, Hengshuihe, and Jinlinghe River Basins—and analyzed five geomorphic indices. The spatial resolution of the data is 30 m. Our conclusions are as follows:

(1) Various geomorphic indices indicate that the LBFZ has experienced relatively high tectonic activity. The geomorphological response to the tectonic activity and relative uplift of the LBFZ include rivers with generally high SL/K values, drainage basins with relatively high HI and low Re (elongated) values, basins with different degrees of asymmetry (AF), and leading edges of mountains with low VF values.

(2) The tectonic tilt direction of the region shows regional zoning on both sides of the fault zone. These indicate that

https://doi.org/10.1007/s12303-023-0023-8

tectonic activity has influenced the evolution of the watershed in this area. Meanwhile, the morphology and AF values of the drainage basin on the southwest side of the study area indicate the influence of northwest-southeast compressive stress.

(3) Tectonic activity of the LQF is the highest in the area, followed by that of the TGF; the activity of the GGF is weak, and the QBF is the lowest. For each fault, the activity level varies along the strike.

(4) The northeastward expansion of the Tibetan Plateau affected the LBFZ region, and the stress brought about by it controlled the tectonic deformation in the region and also sculpted the modern landscape.

ACKNOWLEDGMENTS

We gratefully acknowledge the detailed comments and suggestions by two anonymous journal reviewers, which improved the manuscript. We also appreciate Professor J.V. Pérez-Peña for his tool provided, and the significant help from Dr. Mengyue Duan during the fieldwork. This study was co-funded by Natural Science Basic Research Project in Shaanxi Province (No. 2022JM-162), Doctoral Research Start-up Fund Project in Yulin University (22GK12), and Science and Technology Program in Yulin (CXY-2021-110-02).

REFERENCES

Azañón, J.M., Pérez-Peña, J.V., Giaconia, F., Booth-Rea, G., Martínez-Martínez, J.M., and Rodríguez-Peces, M.J., 2012, Active tectonics in the central and eastern Betic Cordillera through morphotectonic analysis: the case of Sierra Nevada and Sierra Alhamilla. Journal of Iberian Geology, 38, 225–238. https://doi.org/10.5209/rev_JIGE.2012.v38.n1.39214

Brocklehurst, S.H. and Whipple, K.X., 2004, Hypsometry of glaciated landscapes. Earth Surface Processes and Landforms, 29, 907–926. https://doi.org/10.1002/esp.1083

Brookfield, M.E., 1998, The evolution of the great river systems of southern Asia during the Cenozoic India-Asia collision: rivers draining southwards. Geomorphology, 22, 285–312. https://doi.org/10.1016/S0169-555X(97)00082-2

Bull, W.B., 1978, Geomorphic tectonic class of the south front of the San Gabriel Mountains. USGS Contract Report, 14-08-001-G-394, U.S. Geological Survey, Office of Earthquakes, Volcanoes and Engineering, Menlo Park, USA, 188 p.

Bull, W.B., 2007, Tectonic Geomorphology of Mountains: A New Approach to Paleoseismology. Blackwell, Malden, USA, 316 p.

Bull, W.B., 2009, Tectonically Active Landscapes. Wiley-Blackwell, Chichester, UK, 326 p.

Bull, W.B. and Mcfadden, L.D., 1977, Tectonic geomorphology north and south of the Garlock fault, California. Proceedings of the 8th Annual Geomorphology Symposium on Geomorphology in Arid Regions, State University of New York, Binghamton, USA, Sep. 23–24, p. 115–138.

Burbank, D.W. and Anderson, R.S., 2012, Tectonic Geomorphology (2nd edition). Wiley-Blackwell, Oxford, UK, 454 p.

Bureau of Geology and Mineral Resources of Shaanxi Province, 1989, Regional geology of Shaanxi Province. Geological Publishing House, Beijing, 707 p. (in Chinese).

Canon, P.J., 1976, Generation of explicit parameters for a quantitative geomorphic study of the Mill Creek drainage basin. Oklahoma Geology Notes, 36, 3–17.

Chang, Z.Y., Wang, J., Bai, S.B., and Zhang, Z.G., 2014, Appraisal of active tectonic in Bailongjiang Basin based on DEM data. Quaternary Sciences, 34, 292–301. (in Chinese with English abstract). https://doi.org/10.3969/j.issn.1001-7410.2014.02.03

Chen, Q.Y., Xiong, R.W., and Tian, Q.J., 2018, Segmentary characteristics of the geometrical structure of the Longxian-Qishan-Mazhao Active Fault. Earthquake, 38, 66–80. (in Chinese with English abstract). https://doi.org/10.3969/j.issn.1000-3274.2018.03.007

Chen, S.E., Fan, S.H., Wang, X.Z., Wang, R.P., Liu, Y.L., Yang L.C., Ning, X.H., and Li, R.X., 2018, Neotectonic movement in the southern margin of the Ordos Block inferred from the Qianhe River terraces near the north of the Qinghai-Tibet Plateau. Geological Journal, 53, 274–281. https://doi.org/10.1002/gj.3111

Chen, Y.-C., Sung, Q., and Cheng, K.-Y., 2003, Along-strike variations of morphotectonic features in the Western Foothills of Taiwan: tectonic implications based on stream-gradient and hypsometric analysis. Geomorphology, 56, 109–137. https://doi.org/10.1016/S0169-555X(03)00059-X

Cheng, K.-Y., Hung, J.-H., Chang, H.-C., Tsai, H., and Sung, Q.-C., 2012, Scale independence of basin hypsometry and steady state topography. Geomorphology, 171–172, 1–11. https://doi.org/10.1016/j.geomorph.2012.04.022

Cheng, W.M., Wang, N., Zhao, M., and Zhao, S.M., 2016, Relative tectonics and debris flow hazards in the Beijing mountain area from DEM-derived geomorphic indices and drainage analysis. Geomorphology, 257, 134–142. https://doi.org/10.1016/j.geomorph.2016.01.003

Cheng, Y.L., He, C.Q., Rao, G., Yan, B., Lin, A.M., Hu, J.M., Yu, Y.L., and Yao, Q., 2018, Geomorphological and structural characterization of the southern Weihe Graben, central China: implications for fault segmentation. Tectonophysics, 722, 11–24. https://doi.org/10.1016/j.tecto.2017.10.024

Cox, R.T., 1994, Analysis of drainage-basin symmetry as a rapid technique to identify areas of possible Quaternary tilt-block tectonics: an example from the Mississippi Embayment. GSA Bulletin, 106, 571–581. https://doi.org/10.1130/0016-7606(1994)106<0571:AODBSA>2.3.CO;2

Cuong, N.Q. and Zuchiewicz, W.A., 2001, Morphotectonic properties of the Lo River Fault near Tam Dao in North Vietnam. Natural Hazards and Earth System Sciences, 1, 15–22. https://doi.org/10.5194/nhess-1-15-2001

Dai, H.B. and Tang, H.T., 2021, Analysis of tectonic stress field characteristics of Longxian–Baoji Fault Zone based on GPS data. Journal of Geodesy and Geodynamics, 41, 413–418. (in Chinese with English abstract). https://doi.org/10.14075/j.jgg.2021.04.017

Dai, Y., Wang, X.Y., Wang, S.L., Li, Y.Q., and Lu, H.Y., 2016, The neotectonic activity of Wanchuan catchment reflected by geomorphic

indices. Acta Geographica Sinica, 71, 412–421. (in Chinese with English abstract). https://doi.org/10.11821/dlxb201603005

Dar, R.A., Romshoo, S.A., Chandra, R., and Ahmad, I., 2014, Tectono-geomorphic study of the Karewa Basin of Kashmir Valley. Journal of Asian Earth Sciences, 92, 143–156. https://doi.org/10.1016/j.jseaes.2014.06.018

Davis, W.M., 1899, The Geographical cycle. Geographical Journal, 14, 481–504. https://doi.org/10.2307/1774538

Dehbozorgi, M., Pourkermani, M., Arian, M., Matkan, A.A., Motamedi, H., and Hosseiniasl, A., 2010, Quantitative analysis of relative tectonic activity in the Sarvestan area, central Zagros, Iran. Geomorphology, 121, 329–341. https://doi.org/10.1016/j.geomorph.2010.05.002

Dey, S., Kaushal, R.K., Sonam, and Jain, V., 2019, Spatiotemporal variability of neotectonic activity along the Southern Himalayan front: a geomorphic perspective. Journal of Geodynamics, 129, 237–246. https://doi.org/10.1016/j.jog.2018.09.003

Domínguez-González, L., Andreani, L., Stanek, K.P., and Gloaguen, R., 2015, Geomorpho-tectonic evolution of the Jamaican restraining bend. Geomorphology, 228, 320–334. https://doi.org/10.1016/j.geomorph.2014.09.019

Dumka, R.K., Kotlia, B.S., Suribabu, D., Narain, P., and Prajapati, S., 2019, Present-day crustal deformation and geodetic strain in the vicinity of Dholavira – Harappan civilization site, Kachchh, western part of the Indian plate. Quaternary International, 507, 324–332. https://doi.org/10.1016/j.quaint.2018.10.035

El Hamdouni, R., Irigaray, C., Fernández, T., Chacón, J., and Keller, E.A., 2008, Assessment of relative active tectonics, southwest border of the Sierra Nevada (southern Spain). Geomorphology, 96, 150–173. https://doi.org/10.1016/j.geomorph.2007.08.004

Erbello, A., Melnick, D., Zeilinger, G., Bookhagen, B., Pingel, H., and Strecker, M.R., 2022, Geomorphic expression of a tectonically active rift-transfer zone in southern Ethiopia. Geomorphology, 403, 108162. https://doi.org/10.1016/j.geomorph.2022.108162

Faghih, A., Nezamzadeh, I., and Kusky, T.M., 2016, Geomorphometric evidence of an active pop-up structure along the sabzpushan fault zone, Zagros mountains, SW Iran. Journal of Earth Science, 27, 945–954. https://doi.org/10.1007/s12583-016-0663-y

Fan, S.H., Zhang, T.Y., Lu, Y.D., and Chen, S.E., 2020, Quantitative analysis of morphotectonic features of the Longxian-Qishan Fault in the southwestern margin of Ordos Block. Northwestern Geology, 53, 60–76. (in Chinese with English abstract) https://doi.org/10.19751/j.cnki.61-1149/p.2020.02.004

Fang, X.M., 2017, Uplift stage of the Tibetan Plateau. Science & Technology Review, 35, 42–50. (in Chinese with English abstract).

Farr, T.G. and Kobrick, M., 2000, Shuttle radar topography mission produces a wealth of data. Eos, Transactions American Geophysical Union, 81, 583–585. https://doi.org/10.1029/eo081i048p00583

Figueiredo, P.M., Rockwell, T.K., Cabral, J., and Cristina, P.L., 2019, Morphotectonics in a low tectonic rate area: analysis of the southern Portuguese Atlantic coastal region. Geomorphology, 326, 132–151. https://doi.org/10.1016/j.geomorph.2018.02.019

Gao, M.X., Zeilinger, G., Xu, X.W., Wang, Q.L., and Hao, M., 2013, DEM and GIS analysis of geomorphic indices for evaluating recent uplift of the northeastern margin of the Tibetan Plateau, China. Geomorphology, 190, 61–72. https://doi.org/10.1016/j.geomorph.2013.02.008

Gardner, T.W., Back, W., Bullard, T.F., Hare, P.W., Kesel, R.H., Lowe, D.R., Menges, C.M., Mora, S.C., Pazzaglia, F.J., Sasowsky, I.D., Troester, J.W., and Wells, S.G., 1987, Central America and the Caribbean. In: Graf, W.L. (ed.), Geomorphic Systems of North America. Centennial Special Volumes, Geological Society of America, 2, p. 343–401. https://doi.org/10.1130/DNAG-CENT-v2.343

Ghosh, S. and Sivakumar, R., 2018, Assessment of morphometric parameters for the development of Relative Active Tectonic Index and its significant for seismic hazard study: an integrated geoinformatic approach. Environmental Earth Sciences, 77, 600. https://doi.org/10.1007/s12665-018-7787-6

Giano, S.I., Pescatore, E., Agosta, F., and Prosser, G., 2018, Geomorphic evidence of Quaternary tectonics within an underlap fault zone of southern Apennines, Italy. Geomorphology, 303, 172–190. https://doi.org/10.1016/j.geomorph.2017.11.020

Gimenez, V.B., Salamuni, E., and Dos Santos, J.M., 2022, The role of fault reactivation in the geomorphological evolution of coastal landforms on passive continental margins: evidence from a tectonic estuary in southern Brazil. Geomorphology, 402, 108132. https://doi.org/10.1016/j.geomorph.2022.108132

Graveleau, F., Strak, V., Dominguez, S., Malavieille, J., Chatton, M., Manighetti, I., and Petit, C., 2015, Experimental modelling of tectonics-erosion-sedimentation interactions in compressional, extensional, and strike-slip settings. Geomorphology, 244, 146–168. https://doi.org/10.1016/j.geomorph.2015.02.011

Grohmann C.H., 2004, Morphometric analysis in geographic information systems: applications of free software GRASS and R. Computers & Geosciences, 30, 1055–1067. https://doi.org/10.1016/j.cageo.2004.08.002

Guan, X., Pang, L.C., Jiang, Y.T., Lv, H.H., and Zheng, X.M., 2021, Spatial characteristics of quantitative geomorphic indices in the Taihang Mountains, north China: implications for tectonic geomorphology. Journal of Geomechanics, 27, 280–293. (in Chinese with English abstract) https://doi.org/10.12090/j.issn.1006-6616.2021.27.02.026

Guo, S.S., Hao, M., and Zhu, Y.Q., 2012, Gravity evidence of underplating in the northeastern margin area of Qinghai-Tibet plateau. Geodesy and Geodynamics, 3, 46–50. https://doi.org/10.3724/SP.J.1246.2012.00046

Gupta, L., Agrawal, N., Dixit, J., and Dutta, S., 2022, A GIS-based assessment of active tectonics from morphometric parameters and geomorphic indices of Assam Region, India. Journal of Asian Earth Sciences: X, 8, 100115. https://doi.org/10.1016/j.jaesx.2022.100115

Hack, J.T., 1973, Stream-profiles analysis and stream-gradient index. Journal of Research of the U.S. Geological Survey, 1, 421–429.

Hare, P.W. and Gardner, T.W., 1985, Geomorphic indicators of vertical neotectonism along converging plate margins, Nicoya Peninsula, Costa Rica. In: Morisawa, M. and Hack, J.T. (eds.), Tectonic Geomorphology. Proceedings of the 15th Annual Binghamton Geomorphology Symposium, Allen and Unwin, Boston, USA, p. 75–104.

Hurtrez, J.-E., Sol, C., and Lucazeau, F., 1999, Effect of drainage area on hypsometry from an analysis of small-scale drainage basins in the Siwalik Hills (Central Nepal). Earth Surface Processes and Landforms, 24, 799–808. https://doi.org/10.1002/(SICI)1096-9837(199908)24:9<799::AID-ESP12>3.0.CO;2-4

Keller, E.A., 1986, Investigation of active tectonics: use of surficial earth processes. In: Geophysics Study Committee, Geophysics Research

Forum, Commission on Physical Sciences, Mathematics, and Resources, National Research Council (eds.), Active Tectonics: Impact on Society. Studies in Geophysics, National Academy Press, Washington DC, USA, p. 136–147.

Keller, E.A. and Pinter, N., 2002, Active Tectonics: Earthquakes, Uplift and Landscape (2nd edition). Prentice Hall, Upper Saddle River, USA, 362 p.

Keller, E.A. and Rockwell, T.K., 1984, Tectonic geomorphology, Quaternary chronology, and paleoseismicity. In: Costa, J.E. and Fleisher, P.J. (eds.), Developments and Applications of Geomorphology. Springer, Berlin, Germany, p. 203–239. https://doi.org/10.1007/978-3-642-69759-3_7

Kirby, E. and Whipple, K.X., 2012, Expression of active tectonics in erosional landscapes. Journal of Structural Geology, 44, 54–75. https://doi.org/10.1016/j.jsg.2012.07.009

Kothyari, G.C., Rastogi, B.K., Morthekai, P., Dumka, R.K., and Kandregula, R.S., 2016, Active segmentation assessment of the tectonically active South Wagad Fault in Kachchh, Western Peninsular India. Geomorphology, 253, 491–507. https://doi.org/10.1016/j.geomorph.2015.10.029

Kumar, N., Dumka, R.K., Mohan, K., and Chopra, S., 2022, Relative active tectonics evaluation using geomorphic and drainage indices, in Dadra and Nagar Haveli, western India. Geodesy and Geodynamics, 13, 219–229. https://doi.org/10.1016/j.geog.2022.01.001

Lei, Q.Y., Zhang, P.Z., Zheng, W.J., Chai, C.Z., Wang, W.T., Du, P., and Yu, J.X., 2016, Dextral strike-slip of Sanguankou–Niushoushan fault zone and extension of arc tectonic belt in the northeastern margin of the Tibet Plateau. Science China Earth Sciences, 59, 1025–1040. https://doi.org/10.1007/s11430-016-5272-1

Li, H.P., Chen, J.L., and Zhang, Z.W., 2004, The regional geological survey reports of 1: 250000 Baoji City. Shaanxi Institute of Geological Survey, Xian, China, 337 p. (in Chinese with English abstract)

Li, X.N., 2017, Deformation pattern based on geometry and kinematics of active tectonics in the southwestern Ordos Block. Ph.D. Thesis, Institute of Geology, China Earthquake Administration, Beijing, China, 128 p. (in Chinese with English abstract)

Li, X.N., Feng, X.J., Li, X.N., Li, C.Y., Zheng, W.J., Zhang, P.Z., Pierce, I.K.D., Li, G.Y., Li, C.X., Liu, Y.J., Ren, G.X., and Luo, Q.X., 2019, Geological and geomorphological evidence for active faulting of the southern Liupanshan fault zone, NE Tibetan Plateau. Geomorphology, 345, 106849. https://doi.org/10.1016/j.geomorph.2019.106849

Li, X.N., Pierce, I.K.D., Ai, M., Luo, Q., Li, C.Y., Zheng, W.J., and Zhang, P.Z., 2022, Active tectonics and landform evolution in the Longxian–Baoji Fault Zone, Northeast Tibet, China, determined using combined ridge and stream profiles. Geomorphology, 410, 108279. https://doi.org/10.1016/j.geomorph.2022.108279

Li, X.N., Zhang, P.Z., Zheng, W.J., Feng, X.J., Li, C.Y., Pierce, I.K.D., Xu, H.Y., Li, X.N., Ai, M., Chen, G., Dong, J.Y., Liu, J.R., and Ren, G.X., 2018, Kinematics of Late Quaternary slip along the Qishan-Mazhao Fault: implications for tectonic deformation on the southwestern Ordos, China. Tectonics, 37, 2983–3000. https://doi.org/10.1029/2018TC005043

Li, Y.H., Liu, M., Wang, Q.L., and Cui, D.X., 2018, Present-day crustal deformation and strain transfer in northeastern Tibetan Plateau. Earth and Planetary Science Letters, 487, 178–189. https://doi.org/10.1016/j.epsl.2018.01.024

Lifton, N.A. and Chase, C.G., 1992, Tectonic, climatic and lithologic influences on landscape fractal dimension and hypsometry: implications for landscape evolution in the San Gabriel Mountains, California. Geomorphology, 5, 77–114. https://doi.org/10.1016/0169-555X(92)90059-W

Lin, A.M., Rao, G., and Yan, B., 2015, Flexural fold structures and active faults in the northern-western Weihe Graben, central China. Journal of Asian Earth Sciences, 114, 226–241. https://doi.org/10.1016/j.jseaes.2015.04.012

Liu, C.Y., Zhao, H.G., Gui, X.J., Yue, L.P., Zhao, J.F., and Wang, J.Q., 2006, Space-time coordinate of the evolution and reformation and mineralization response in Ordos Basin. Acta Geologica Sinica, 80, 617–638. (in Chinese with English abstract) https://doi.org/10.3321/j.issn:0001-5717.2006.05.001

Liu, H.Y., 2017, Geomorphic indexes extracting method and its relationship with tectonic activities—a case study of the south segment of Longmenshan Fault Belt. Resources Environment & Engineering, 31, 343–351. (in Chinese with English abstract) https://doi.org/10.16536/j.cnki.issn.1671-1211.2017.03.022

Liu, J., Zhang, J.Y., Ge, Y.K., Wang, W., Zeng, L.X., Li, G., and Lin, X., 2018, Tectonic geomorphology: an interdisciplinary study of the interaction among tectonic climatic and surface processes. Chinese Science Bulletin, 63, 3070–3088. (in Chinese with English abstract) https://doi.org/10.1360/N972018-00498

Liu, S.W., Gan, J.S., Yao, Y.S., and Shen, C.Y., 1997, Strike-slip transformation deformation along the northern boundary fault of western Qinling MT and Haiyuan Fault and interaction between them and Longshan Block. Crustal Deformation and Earthquake, 17, 73–83. (in Chinese with English abstract)

Liu, Z.H., Han, L., Boulton, S.J., Wu, T.T., and Guo, J.H., 2020, Quantifying the transient landscape response to active faulting using fluvial geomorphic analysis in the Qianhe Graben on the southwest margin of Ordos, China. Geomorphology, 351, 106974. https://doi.org/10.1016/j.geomorph.2019.106974

Mahmood, S.A. and Gloaguen, R., 2012, Appraisal of active tectonics in Hindu Kush: insights from DEM derived geomorphic indices and drainage analysis. Geoscience Frontiers, 3, 407–428. https://doi.org/10.1016/j.gsf.2011.12.002

Mayer, L., 1990, Introduction to Quantitative Geomorphology: An Exercise Manual. Prentice Hall, Englewood Cliffs, USA, 384 p.

Meyer, B., Tapponnier, P., Bourjot, L., Métivier, F., Gaudemer, Y., Peltzer, G., Guo, S.M., and Chen, Z.T., 1998, Crustal thickening in Gansu-Qinghai, lithospheric mantle subduction, and oblique, strike-slip controlled growth of the Tibet Plateau. Geophysical Journal International, 135, 1–47. https://doi.org/10.1046/j.1365-246X.1998.00567.x

Molnar, P. and Tapponnier, P., 1975, Cenozoic tectonics of Asia: effects of a continental collision: features of recent continental tectonics in Asia can be interpreted as results of the India-Eurasia collision. Science, 189, 419–426. https://doi.org/10.1126/science.189.4201.419

Monteiro, K.A., Missura, R., and Correa, A.C.B., 2010, Application of the hack index – or stream length-gradient index (SL index) – to the Tracunhaem River Watershed, Pernambuco, Brazil. Geociências, 29, 533–539.

Ntokos, D., Lykoudi, E., and Rondoyanni, T., 2016, Geomorphic analysis

in areas of low-rate neotectonic deformation: South Epirus (Greece) as a case study. Geomorphology, 263, 156–169. https://doi.org/10.1016/j.geomorph.2016.04.005

Ohmori, H., 1993, Changes in the hypsometric curve through mountain building resulting from concurrent tectonics and denudation. Geomorphology, 8, 263–277. https://doi.org/10.1016/0169-555X(93)90023-U

Pedrera, A., Pérez-Peña, J.V., Galindo-Zaldívar, J., Azañón, J.M., and Azor, A., 2009, Testing the sensitivity of geomorphic indices in areas of low-rate active folding (eastern Betic Cordillera, Spain). Geomorphology, 105, 218–231. https://doi.org/10.1016/j.geomorph.2008.09.026

Pei, X., Li, Z.H., and Shi, Y., 2021, Formation mechanism of arcuate tectonic structures around northeast Tibetan Plateau: insight from 3-D numerical modeling. Terra Nova, 33, 345–355. https://doi.org/10.1111/ter.12519

Peltzer, G., Tapponnier, P., and Armijo, R., 1989, Magnitude of late quaternary left-lateral displacements along the north edge of Tibet. Science, 246, 1285–1289. https://doi.org/10.1126/science.246.4935.1285

Pérez-Peña, J.V., Azañón, J.M., and Azor, A., 2009a, CalHypso: an ArcGIS extension to calculate hypsometric curves and their statistical moments. Applications to drainage basin analysis in SE Spain. Computers & Geosciences, 35, 1214–1223. https://doi.org/10.1016/j.cageo.2008.06.006

Pérez-Peña, J.V., Azañón, J.M., Azor, A., Delgado, J., and González-Lodeiro, F., 2009b, Spatial analysis of stream power using GIS: SLk anomaly maps. Earth Surface Processes and Landforms, 34, 16–25. https://doi.org/10.1002/esp.1684

Pérez-Peña, J.V., Azor, A., Azañón, J.M., and Keller, E.A., 2010, Active tectonics in the Sierra Nevada (Betic Cordillera, SE Spain): insights from geomorphic indexes and drainage pattern analysis. Geomorphology, 119, 74–87. https://doi.org/10.1016/j.geomorph.2010.02.020

Pike, R.J. and Wilson, S.E., 1971, Elevation-relief ratio, hypsometric integral, and geomorphic area-altitude analysis. GSA Bulletin, 82, 1079–1084. https://doi.org/10.1130/0016-7606(1971)82[1079:ERHIAG]2.0.CO;2

Ramírez-Herrera, M.T., 1998, Geomorphic assessment of active tectonics in the Acambay graben, Mexican Volcanic Belt. Earth Surface Processes and Landforms, 23, 317–332. https://doi.org/10.1002/(SICI)1096-9837(199804)23:4<317::AID-ESP845>3.0.CO;2-V

Regard, V., Lagnous, R., Espurt, N., Darrozes, J., Baby, P., Roddaz, M., Calderon, Y., Hermoza, W., 2009, Geomorphic evidence for recent uplift of the Fitzcarrald Arch (Peru): a response to the Nazca Ridge subduction. Geomorphology, 107, 107–117. https://doi.org/10.1016/j.geomorph.2008.12.003

Rimando, J.M. and Schoenbohm, L.M., 2020, Regional relative tectonic activity of structures in the Pampean flat slab segment of Argentina from 30 to 32°S. Geomorphology, 350, 106908. https://doi.org/10.1016/j.geomorph.2019.106908

Rockwell, T.K., Keller, E.A., and Johnson, D.L., 1985, Tectonic geomorphology of alluvial fans and mountain fronts near Ventura, California. In: Morisawa, M. and Hack, J.T. (eds.), Tectonic Geomorphology. Proceedings of the 15th Annual Binghamton Geomorphology Symposium, Allen and Unwin, Boston, USA, p. 183–207.

Royden, L.H., Burchfiel, B.C., and van der Hilst, R.D., 2008, The geological evolution of the Tibetan Plateau. Science, 321, 1054–1058. https://doi.org/10.1126/science.1155371

Schumm, S.A., 1956, Evolution of drainage systems and slopes in Badlands at Perth Amboy, New Jersey. GSA Bulletin, 67, 597–646. https://doi.org/10.1130/0016-7606(1956)67[597:EODSAS]2.0.CO;2

Seeber, L. and Gornitz, V., 1983, River profiles along the Himalayan arc as indicators of active tectonics. Tectonophysics, 92, 335–367. https://doi.org/10.1016/0040-1951(83)90201-9

Seong, Y.B., Owen, L.A., Bishop, M.P., Bush, A., Clendon, P., Copland, L., Finkel, R.C., Kamp, U., and Shroder, J.F., 2008, Rates of fluvial bedrock incision within an actively uplifting orogen: central Karakoram Mountains, northern Pakistan. Geomorphology, 97, 274–286. https://doi.org/10.1016/j.geomorph.2007.08.011

Shi, X.H., Yang, Z., Dong, Y.P., Qu, H.J., Zhou, B., and Cheng, B., 2020, Geomorphic indices and longitudinal profile of the Daba Shan, northeastern Sichuan Basin: evidence for the late Cenozoic eastward growth of the Tibetan Plateau. Geomorphology, 353, 107031. https://doi.org/10.1016/j.geomorph.2020.107031

Shi, X.H., Yang, Z., Dong, Y.P., and Zhou, B., 2019, Tectonic uplift of the northern Qinling Mountains (central China) during the late Cenozoic: evidence from DEM-based geomorphological analysis. Journal of Asian Earth Sciences, 184, 104005. https://doi.org/10.1016/j.jseaes.2019.104005

Shi, Z.G., Yuan, D.Y., He, W.G., Liu, X.W., and Wang, J., 2015, Recent activity of the Badu-Longwei segment, Guguan-Xiangong fault in southern Liupanshan, constrained by rhythmic sediment lithology and geomorphic characteristics. Acta Geologica Sinica (English Edition), 89, 1165–1175. https://doi.org/10.1111/1755-6724.12521

Silva, P.G., Goy, J.L., Zazo, C., and Bardají, T., 2003, Fault-generated mountain fronts in southeast Spain: geomorphologic assessment of tectonic and seismic activity. Geomorphology, 50, 203–225. https://doi.org/10.1016/S0169-555X(02)00215-5

State Seismological Bureau Research Group (SSBRG), 1988, Active Fault System around the Ordos. Seismological Press, Beijing, China, 355 p. (in Chinese).

Strahler, A.N., 1952, Hypsometric (area-altitude) analysis of erosional topography. GSA Bulletin, 63, 1117–1142. https://doi.org/10.1130/0016-7606(1952)63[1117:HAAOET]2.0.CO;2

Strahler, A.N., 1964, Quantitative geomorphology of drainage basins and channel networks. In: Chow, V.T. (ed.), Handbook of Applied Hydrology. McGraw Hill Book Company, New York, USA, p. 439–476.

Su, Q., Yuan, D.Y., Xie, H., Shao, Y.X., and Liang, M.J., 2016, Geomorphic features of the Shule River Brainage Basin in Qilianshan and its insight into tectonic implications. Seismology and Geology, 38, 240–258. (in Chinese with English abstract) https://doi.org/10.3969/j.issn.0253-4967.2016.02.002

Summerfield, M.A., 2000, Geomorphology and Global Tectonics. John Wiley & Sons, Chichester, UK, 386 p.

Sun, Z.M. and Deng, Q.D., 1994, Basic characteristics and interaction of the eastern Liupanshan piedmont fault and the Longxian–Baoji Fault Zone. In: Seismogeology Professional Committee and Seismological Society of China (eds.), Active Faults Research in China. Seismological Press, Beijing, p. 114–125. (in Chinese).

Tang, Y.C., Zhou, S.Y., Chen, Y.J, Sandvol, E., Liang, X.F., Feng, Y., Jin, G., Jiang, M.M., and Liu, M., 2015, Crustal structures across the western

Weihe Graben, North China: implications for extrusion tectonics at the northeast margin of Tibetan Plateau. Journal of Geophysical Research: Solid Earth, 120, 5070–5081. https://doi.org/10.1002/2014JB011210

Tapponnier, P., Xu, Z.Q., Roger, F., Meyer, B., Arnaud, N., Wittlinger, G., and Yang, J.S., 2001, Oblique stepwise rise and growth of the Tibet Plateau. Science, 294, 1671–1677. https://doi.org/10.1126/science.105978

Troiani, F. and Della Seta, M., 2008, The use of the stream length-gradient index in morphotectonic analysis of small catchments: a case study from central Italy. Geomorphology, 102, 159–168. https://doi.org/10.1016/j.geomorph.2007.06.020

Tsodoulos, I.M., Koukouvelas, I.K., and Pavlides, S., 2008, Tectonic geomorphology of the easternmost extension of the Gulf of Corinth (Beotia, Central Greece). Tectonophysics, 453, 211–232. https://doi.org/10.1016/j.tecto.2007.06.015

Wang, A. and Wang, G.C., 2005, Review on morphotectonic and its analytical methods. Bulletin of Geological Science and Technology, 24, 7–20. (in Chinese with English abstract) https://doi.org/10.3969/j.issn.1000-7849.2005.04.002

Wang, M. and Shen, Z.-K., 2020, Present-day crustal deformation of continental China derived from GPS and its tectonic implications. Journal of Geophysical Research: Solid Earth, 125, e2019JB018774. https://doi.org/10.1029/2019JB018774

Wang, S.D., Shi, Y.Q., and Dong, Y.P., 2018, The active characteristics in the Quaternary period of the middle Guguan-Guozhen fault, northeast margin of Qinghai-Tibet Plateau. Chinese Journal of Geology, 53, 781–798. (in Chinese with English abstract) https://doi.org/10.12017/dzkx.2018.044

Wang, S.D., Shi, Y.Q., Feng, X.J., and Tian, Z., 2021, Late Quaternary sinistral strike-slipping of the Liupanshan–Baoji fault zone: implications for the growth of the northeastern Tibetan Plateau. Geomorphology, 380, 107628. https://doi.org/10.1016/j.geomorph.2021.107628

Wang, W.T., Kirby, E., Zhang, P.Z., Zheng, D.W., Zhang, G.L., Zhang, H.P., Zheng, W.J., and Chai, C.Z., 2013, Tertiary basin evolution along the northeastern margin of the Tibetan Plateau: evidence for basin formation during Oligocene transtension. GSA Bulletin, 125, 377–400. https://doi.org/10.1130/B30611.1

Wang, W.T., Zhang, P.Z., Zheng, D.W., and Pang, J.Z., 2014, Late Cenozoic tectonic deformation of the Haiyuan Fault Zone in the northeastern margin of the Tibetan Plateau. Earth Science Frontiers, 21, 266–274. (in Chinese with English abstract) https://doi.org/10.13745/j.esf.2014.04.027

Wang, Z.Y., Fu, G.Y., and She, Y.W., 2018, Crustal density structure, lithosphere flexure mechanism, and isostatic state throughout the Qinling Orogen revealed by in situ dense gravity observations. Journal of Geophysical Research: Solid Earth, 123, 10026–10039. https://doi.org/10.1029/2018JB016117

Weissel, J.K., Pratson, L.F., and Malinverno, A., 1994, The length-scaling properties of topography. Journal of Geophysical Research, 99, 13997–14012. https://doi.org/10.1029/94JB00130

Wells, S.G., Bullard, T.F., Menges, C.M., Drake, P.G., Karas, P.A., Kelson, K.I., Ritter, J.B., and Wesling, J.R., 1988, Regional variations in tectonic geomorphology along a segmented convergent plate boundary pacific coast of Costa Rica. Geomorphology, 1, 239–265. https://doi.org/10.1016/0169-555X(88)90016-5

Willgoose, G. and Hancock, G., 1998, Revisiting the hypsometric curve as an indicator of form and process in transport-limited catchment. Earth Surface Processes and Landforms, 23, 611–623. https://doi.org/10.1002/(SICI)1096-9837(199807)23:7<611::AID-ESP872>3.0.CO; 2-Y

Wu, L., Xiao, A.C., and Yang, S.F., 2014, Impact of wind erosion on detecting active tectonics from geomorphic indexes in extremely arid areas: a case study from the Hero Range, Qaidam Basin, NW China. Geomorphology, 224, 39–54. https://doi.org/10.1016/j.geomorph.2014.07.010

Xu, Y.R., He, H.L., Deng, Q.D., Wei, Z.Y., Bi, L.S., and Sun, H.Y., 2013, Quantitative river geomorphic parameters surrounding MTS. Huoshan, Shanxi Province and their tectonic implications. Quaternary Sciences, 33, 746–759. (in Chinese with English abstract) https://doi.org/10.3969/j.issn.1001-7410.2013.04.12

Yang, Y., Qin, X., Shi, W., Zhang, Y., and Zhao, Z.X., 2022, Segmentation of the active Liumugao Fault, NE Tibetan Plateau as revealed by DEM-derived geomorphic indices. Geosystems and Geoenvironment, 1, 100056. https://doi.org/10.1016/j.geogeo.2022.100056

Yang, Y.H., Zhang, X.M., Dong, Y.P., Sun, S.S., Hua, Q., and Liang, C.T., 2022, Crustal deformation patterns in the Tibetan Plateau and its adjacent regions as revealed by receiver functions. Bulletin of the Seismological Society of America, 112, 1297–1314. https://doi.org/10.1785/0120210228

Yin, A. and Harrison, M., 2000, Geological evolution of the Himalayan Tibetan orogen. Annual Review of Earth and Planetary Sciences, 28, 211–280. https://doi.org/10.1146/annurev.earth.28.1.211

Yu, Q., Ren, Z.L., Li, R.X., Chung, L., Tao, Ni., Cui, J.P., Wang, B.J., Qi, K., and Khaled, A., 2021, Cooling history of the southwestern Ordos Basin (northern China) since Late Jurassic: insights from thermochronology and geothermometry. Journal of Asian Earth Sciences, 219, 104895. https://doi.org/10.1016/j.jseaes.2021.104895

Yuan, D.Y., Ge, W.P., Chen, Z.W., Li, C.Y., Wang, Z.C., Zhang, H.P., Zhang, P.Z., Zheng, D.W., Zheng, W.J., Craddock, W.H., Dayem, K.E., Duvall, A.R., Hough, B.G., Lease, R.O., Champagnac, J.-D., Burbank, D.W., Clark, M.K., Farley, K.A., Garzione, C.N., Kirby, E., Molnar, P., and Roe, G.H., 2013, The growth of northeastern Tibet and its relevance to large-scale continental geodynamics: a review of recent studies. Tectonics, 32, 1358–1370. https://doi.org/10.1002/tect.20081

Yuan, D.Y., Zhang, P.Z., Liu, B.C., Gan, W.J., Mao, F.Y., Wang, Z.C., Zheng, W.J., and Guo, H., 2004, Geometrical imagery and tectonic transformation of Late Quaternary active tectonics in northeastern margin of Qinghai-Xizang Plateau. Acta Geologica Sinica, 78, 270–278. (in Chinese with English abstract) https://doi.org/10.3321/j.issn:0001-5717.2004.02.017

Zhang, H.P., Liu, C.C., Xiong, J.G., Pang, J.Z., Yu, J.X., and Wang, Y.Z., 2022, Late Cenozoic tectonic deformation and geomorphological evolution in the Gonghe-Chaka Basin on the northeastern margin of the Tibetan Plateau. Quaternary Sciences, 42, 662–672. (in Chinese with English abstract) https://doi.org/10.11928/j.issn.1001-7410.2022.03.04

Zhang, J.J., Zhu, W.B., Zhao, F., Zhu, L.Q., Li, M.J., Zhu, M., and Zhang, X.D., 2018, Spatial variations of terrain and their impacts on land-

scape patterns in the transition zone from mountains to plains – A case study of Qihe River Basin in the Taihang Mountains. Science China Earth Sciences, 61, 450–461. https://doi.org/10.1007/s11430-016-9158-2

Zhang, P.Z., Burchfiel, B.C., Molnar, P., Zhang, W.Q., Jiao, D.C., Deng, Q.D., Wang, Y.P., Royden, L., and Song, F.M., 1991, Amount and style of late Cenozoic deformation in the Liupan Shan area, Ningxia autonomous region, China. Tectonics, 10, 1111–1129. https://doi.org/10.1029/90TC02686

Zhang, P.Z., Shen, Z.K., Wang, M., Gan, W.J., Bürgmann, R., Molnar, P., Wang, Q., Niu, Z.J., Sun, J.Z., Wu, J.C., Sun, H.R., and You, X.Z., 2004, Continuous deformation of the Tibetan Plateau from global positioning system data. Geology, 32, 809–812. https://doi.org/10.1130/G20554.1

Zhang, T.Q., Wang, Z., Zhang, X.M., Hu, S., Lv, H.H., and Zheng, X.M., 2015, Hypsometric integral analysis of the Urumqi River drainage basin and its implications for topographic evolution. Quaternary Sciences, 35, 60–70. (in Chinese with English abstract) https://doi.org/10.11928/j.issn.1001-7410.2015.01.06

Zhang, T.Y., Fan, S.H., Chen, S.E., Li, S.P., and Lu, Y.D., 2019, Geomorphic evolution and neotectonics of the Qianhe River Basin on the southwest margin of the Ordos Block, North China. Journal of Asian Earth Sciences, 176, 184–195. https://doi.org/10.1016/j.jseaes.2019.02.020

Zhang, X.K., Shao, H.C., and Feng, L.L., 2017, Analysis on seismic in Longxian–Baoji Fault Zone. Plateau Earthquake Research, 29, 19–25. (in Chinese with English abstract) https://doi.org/10.3969/j.issn.1005-586X.2017.01.004

Zhang, Y.Q., Liao, C.Z., Shi, W., and Hu, B., 2006, Neotectonic evolution of the peripheral zones of the Ordos Basin and geodynamic setting. Geological Journal of China Universities, 12, 285–297. (in Chinese with English abstract) https://doi.org/10.3969/j.issn.1006-7493.2006.03.001

Zhang, Y.Q., Mercier, J.L., and Vergély, P., 1998, Extension in the graben systems around the Ordos (China), and its contribution to the extrusion tectonics of South China with respect to Gobi-Mongolia. Tectonophysics, 285, 41–75. https://doi.org/10.1016/S0040-1951(97)00170-4

Zhao, G.H., Li, Y., Yan, Z.K., Yan, L., Li, J.B., Liang, M.J., Ma, C., and Zheng, L.L., 2014, Tectonic geomorphology analysis of piedmont rivers of the middle MT. Longmenshan based on HACK profile and hypsometric integral. Quaternary Sciences, 34, 302–311. (in Chinese with English abstract) https://doi.org/10.3969/j.issn.1001-7410.2014.02.04

Zhao, H.Z., Li, Y.L., and Yang, J.C., 2010, Implication of active structure along the northern Tianshan by stream length-gradient index and Hack profile. Acta Scientiarum Naturalium Universitatis Pekinensis, 46, 237–244. (in Chinese with English abstract) https://doi.org/10.13209/j.0479-8023.2010.034

Zheng, W.J., Yuan, D.Y., Zhang, P.Z., Yu, J.X., Lei, Q.Y., Wang, W.T., Zheng, D.W., Zhang, H.P., Li, X.N., Li, C.Y., and Liu, X.W., 2016, Tectonic geometry and kinematic dissipation of the active faults in the northeastern Tibetan Plateau and their implications for the understanding northeastward growth of the Plateau. Quaternary Sciences, 36, 775–788. (in Chinese with English abstract) https://doi.org/10.11928/j.issn.1001-7410.2016.04.01

Zheng, W.J., Zhang, P.Z., He, W.G., Yuan, D.Y., Shao, Y.X., Zheng, D.W., Ge, W.P., and Min, W., 2013, Transformation of displacement between strike-slip and crustal shortening in the northern margin of the Tibetan Plateau: evidence from decadal GPS measurements and late Quaternary slip rates on faults. Tectonophysics, 584, 267–280. https://doi.org/10.1016/j.tecto.2012.01.006

Zhisheng, A., Kutzbach, J.E., Prell, W.L., and Porter, S.C., 2001, Evolution of Asian monsoons and phased uplift of the Himalaya-Tibetan plateau since Late Miocene times. Nature, 411, 62–66. https://doi.org/10.1038/35075035